INLET MODEL TESTING FACILITY PREPARATION, INJECTOR CALIBRATION AND PRELIMINARY TESTING OF TWO TWO-DIMENSIONAL INLET MODELS AT HIGH INCIDENCE ANGLES TO STUDY INTERNAL FLOW SEPARATION

by

Daniel Robert Hatfield

Thesis submitted to the Graduate Faculty of the
Virginia Polytechnic Institute and State University
in partial fulfillment of the requirements for the degree of
MASTER OF SCIENCE
in
Aerospace and Ocean Engineering

APPROVED:

A. K. Jakubowski, Chairman

J. A. Schetz

G. R. Inger

December, 1978

Blacksburg, Virginia

ACKNOWLEDGEMENTS

I would like to thank . and my other professors for their technical advice and guidance throughout this project. Special thanks, in particular, go to for his correspondence which aided in my finishing this report. Thanks go to my wife, for her patience and understanding while preparing this report.

TABLE OF CONTENTS

NOMENCLATURE

Symbols

A_j	cross sectional injection slot area (measured at slot exit)
C_r	contraction ratio
D	diameter
D_h	highlight diameter
D_{max}	maximum diameter
D_T	throat diameter
L	total length of inlet
L_D	diffuser length
$\dot{m}_i$	mass flow rate of the induced flow
$\dot{m}_j$	mass flow rate of the injected flow
P	static pressure
P_j	injection pressure
P_o	stagnation pressure
P_R	boundary layer rake stagnation pressure
R_x	injector control system variable resistor controls
S_x	injector control system monitoring outputs
T_x	model 12M Scanivalve system's miniature pneumatically operated pressure switch's input/output tubes
T_o	stagnation temperature
V	voltage
α	inlet model incidence angle
α_s	inlet model incidence angle corresponding to internal flow separation

ΔP	dynamic pressure
U_∞	freestream velocity

Subscripts

D	diffuser
F	fan
h	highlight
i	induced
j	injected
o	stagnation
R	boundary layer rake
s	separation
T	throat
x	integer
∞	freestream

LIST OF FIGURES

Page

I. INTRODUCTION

Recently there has been a growing interest in engine inlet design for high angle of attack flow configuration. This interest is especially prevalent in the field of the V/STOL aircraft where the angle of attack of the engine(s) may approach 120°. On commercial aircraft the high angle of attack configuration may occur during take-off and landing when the stagnation streamline can be at an angle of up to 60° with respect to the engine center line [1]. This effect is particularly important for aircraft with engines mounted beneath the wings (Fig. 1).

Depending primarily upon the geometry of the inlet, the angle of attack approaches a limit where internal flow separation occurs (α_s). When separation does occur, large nonuniformities and distortion of the flow at the compressor inlet develop causing decreased performance of the engine, severe mechanical fatigue of the compressor blades, high noise levels, and possible stalling of the engine.

During the past several years NASA Lewis Research Center has been studying the problem of inlet flow separation at high incidence angles. They tested axi-symmetric inlet models which were connected to a small gas turbine engine to produce the flow through the inlet [2,3]. These tests were primarily concerned with the flow field at the compressor face and only limited data was obtained concerning flow separation development. As part of an effort directed at improved understanding of the flow separation mechanisms under various operating conditions, an experimental program has been undertaken at VPI & SU. The program includes wind-tunnel testing of two-dimensional inlet models operated

at various freestream velocities, angles of attack, and inlet mass flow rates. Selection of a 2-D configuration has been motivated mainly by a desire to facilitate application of optical methods for detailed flow observations and photographic recording (Fig. 2)*.

To produce the flow through the inlet a high-pressure injector system had to be designed and built to produce any desired mass flow rate up to the choked flow limit (Fig. 3). Mounting the inlet in the VPI & SU six-foot subsonic stability tunnel allows the simulation of forward speed. The inlet model is mounted to a diffuser and pipe system in such a way that it can be easily inclined at various angles of incidence with respect to the wind-tunnel flow. To test at very high incidence angles, a short section of piping is removed (Fig. 3), the inlet model and adjoining piping is raised, and the inlet model is inclined to a maximum angle of about 60°.

The scope of the work reported in this thesis includes (a) testing, calibration, and selection of the optimal operating parameters of the injector system which serves to drive the air through the inlet models and (b) presentation and discussion of the preliminary results of the inlet models' investigation.

*This report deals primarily with the investigation of the flow by means of pressure data. A full report of the investigation of the flow by means of optical methods will be presented in a thesis authored by Mr. Carl Weiss.

II. INLET TESTING FACILITY

Injector

An injector can be used as an efficient means of inducing fluid flow. The principle of inducing fluid flow is a relatively simple one. A high velocity fluid (injected flow; in this case air) is introduced into a flow field (induced flow). Due to the difference in velocity between the injected and induced flow, the latter is rapidly "energized" and pulled in the direction of the high velocity injected air stream.

Injector design plays an important role in the efficiency of the injector and particularly in the mass-flow efficiency, which can be expressed as the ratio of the mass flow rate of induced air to the mass flow rate of the injected air ($\dot{m}_i/\dot{m}_j$). Two basic injector designs have been known. One utilizes a pipe which extends into the middle of the flow field. High pressure fluid is injected from the pipe into the flow field which induces flow of the surrounding fluid (Fig. 4). The second type utilizes a square duct to contain the flow field. At one station along the duct high pressure fluid is injected into the duct through adjustable slot doors. Thus, there is injected fluid about the perimeter of the duct with variable injection slot area (Fig. 5). This design has one major drawback in that corner flow effects may cause a loss of injector efficiency. The injector design for this study is circular in cross section with high pressure fluid injection about the circumference. Variable injection slot area is achieved through a screw type

mechanism which serves to vary the axial position of an internal "nozzle" section. Turning the screw clockwise closes the injection slot area and turning the screw counterclockwise has the opposite effect (Fig. 6).

High pressure injection air is supplied by a Bury 650 psig compressor and stored in two storage tanks with a total volume of 700 ft^3. An 8 inch butterfly valve with accompanying electro-pneumatic control system regulates the flow of injection air from the storage tanks to the injector (Fig. 7).

Injector Control System

The mass flow rate of induced air is regulated by either changing the pressure of the injected air or changing the injection slot area. These two controlling features are directly related to the injector efficiency which will be discussed in detail in a later section.

Changing the injection slot area is accomplished with two drive motors which can turn the injector screw in either direction. A 40 turn potentiometer is mounted to one of the motor drive shafts to indicate screw position. By applying a voltage across the potentiometer, the variable output can be directly calibrated in terms of the position of the screw and the corresponding injection slot area (Fig. 8). Figure 9 shows the control panel layout for adjusting the injection slot area.

Regulating the injection pressure was accomplished by means of an electro-pneumatic regulator designed and built for this application. The regulator opens the control valve to any desired initial position and then adjusts with time to maintain constant injection pressure

throughout a test run.

The first approach used in designing the electronic control system was to employ a first order feedback loop circuit (Fig. 10)*. Basically the circuit takes an input signal from a pressure transducer on the injector supply line (injected air) and compares it with a signal corresponding to a desired injection pressure. The resulting error signal is inverted and added to the regulating system to correct for any deviation from the input. In principle, this type of feedback loop represents a very effective way for maintaining constant injection pressure. This approach was abandoned because the electronics were faster than the pneumatic response, and control valve oscillations occured which could not be damped out electronically.

The second approach for the electronic control circuit utilizes a pressure transducer generated ramp function signal of the falling storage tank pressure*. This signal is inverted by the control circuit and summed with a set positive (initial valve opening) voltage. Thus, at the start of a test run, the summed value of voltage causes the control valve to open to a desired initial opening position. As the run continues, the dropping storage tank pressure causes the value of summed voltage to increase thereby further opening the control valve to maintain constant injection pressure during a test run (Fig. 11). This type of system requires some initial runs to be made in order to calibrate the control settings (variable resistors R_1 thru R_4) for a desired constant injection pressure and corresponding constant mass flow rate of induced

*Credit for the design of the electronic circuitry for both electronic control systems goes to Mr. Roy C. Allen of Sounds Fine Inc., Blacksburg, VA.

air. Once a constant injection pressure run has been established, recording of the variable resistor values R_1 thru R_4 will enable the same injection pressure run to be repeated at a later date. Only minor adjustments are required at test time in the variable resistors R_1 thru R_4 to correct for changes in temperature and atmospheric pressure which the control system is referenced to.

Figure 12 shows the control panel layout for the electronic control circuit. R_1 is a gain control for the signal coming from the high pressure storage tank. Changing the setting of R_1 changes the slope and magnitude of the ramp function generated by the falling pressure in the storage tank. R_2 is a variable voltage control which is used to zero the value of the voltage at the summing junction. This should be done with the stop-run switch in the stop position and the storage tank pressure at its initial starting pressure. Summing junction voltage is monitored at the S_2 output. The S_1 output is for monitoring injection pressure. R_3 is a gain control for the signal coming from the summing junction. R_4 is the initial opening variable voltage control and is switched to ground in the stop configuration. When switched to run, the initial opening voltage is added in at the summing junction.

Figure 13 shows a typical injection pressure plot for a low or medium mass flow rate through the inlet model. For such conditions, the injection pressure can be kept constant within 3% over a run duration of 20 to 40 seconds. At high mass flow rates, the performance of the pressure regulation system is less adequate and either the useful run is much shorter or some manual adjustments during the run are necessary.

Wind Tunnel

The inlet model tests were conducted in the VPI & SU 6 x 6 foot low speed wind tunnel which is an atmospheric pressure closed-circuit facility with a freestream velocity range of up to 240 ft/sec. Figure 3 shows the inlet model installed in the test section. To vary the angle of attack, the inlet model is rotated in the vertical plane. Small portions of the wind tunnel vertical walls were removed to allow the light beam of the Schlieren Shadowgraph system to pass through the wind tunnel test section.

III. INLET MODELS

Geometry

The inlet models are of modular design which allows for relatively easy change of the lip and diffuser profile geometry (Fig. 2). Two different inlet geometries, designated as Models GE-1 and GE-2, are tested within the framework of this investigation. Figure 14 presents the profiles of the Models GE-1 and GE-2. In general, inlet profiles can be broken down into three separate geometrical shapes: the external forebody, the internal lip and the diffuser.

The external forebody for both inlet models tested is a DAC-1 (Douglas Aircraft Company) series contour (Fig. 15). The internal lip for both inlet models is a 2-to-1 ellipse with contraction ratios of 1.37 and 1.46 for inlet models GE-1 and GE-2, respectively. An identical diffuser was used on both inlet models (Fig. 16).

Instrumentation

The inlet models are instrumented to measure both steady state and fluctuating pressures (Fig. 17). Steady state pressure measurements include static pressures measured along the surface of the windward* profile from the external forebody to the diffuser exit, stagnation pressures obtained from three boundary layer rakes on the windward profile, and a diffuser rake across the diffuser exit. Fluctuating pressure measurements consist of five points along the windward profile surface

*See Figure 2 for a definition of the windward profile.

from the "highlight"* region to the diffuser.

Since detailed information about the separation process in the lip region is desired, it is necessary to place the static pressure ports very close to one another. Small diameter tubing runs underneath the profile surface allowing for the small spacing of the static pressure ports (Fig. 18).

The steady-state pressures are measured by means of four Model 12M Scanivalves having twelve pressure ports each and one Model J Scanivalve with 48 pressure ports. The miniature size of the Model 12M Scanivalves allows mounting them immediately behind the diffuser exit of the inlet model with very short pressure lines between the measuring points and the transducers; thus minimizing response time. The 12M Scanivalves are driven simultaneously by a single miniature D.C. drive motor. The system came equipped with a D.C. gear reduction motor drive assembly which had a constant scanning speed of twelve pressures on each transducer per second. This scanning speed is ideal for use with an electronic data acquisition system where the pressure data can by very quickly stored or recorded. Since it was desired to reproduce the pressure data from the 12M Scanivalve system on strip chart recorders, the scanning speed had to be reduced by a factor of at least four to ensure enough time for the strip chart pens to mechanically respond to each pressure. Reducing the supply voltage to this motor in order to reduce the scanning speed was unsuccessful. For this reason another D.C. gear reduction motor with somewhat slower scanning speed was installed. By varying the supply voltage to this drive motor from zero to a maximum of twenty four volts, the

*See Figure 15 for a definition of the highlight.

scanning speed could be varied from zero to six pressures per second. Setting the supply voltage at approximately eight volts provides a scanning speed of about two pressures per second (for each transducer), and reasonable strip chart response. An additional feature of the 12M Scanivalve system is an encoder assembly which is also driven by the drive motor. The encoder is a rotary switch which is set up to switch on (trigger) when each scanner is in position to connect another pressure port to its transducer. The encoder is designed to be used with a data acquisition system as a triggering device for the taking of pressure data points.

Another important feature of the 12M Scanivalve system is the ZOC (zero-operate-calibrate) feature. The ZOC feature allows for on-line zeroing and calibration of the transducers during actual pressure measurements. The use of miniature pneumatically operated pressure switches allows each transducer to be switched off-line from the model and either some known calibration pressure or a reference pressure to be applied to one of each scanners twelve ports (Fig. 19). To calibrate the transducers, the "calibrate-zero" switch should be in the calibrate position and the "on-off" switch should be in the on position. This allows high pressure air to operate four of the pressure switches; switching from the model to scanner tubes (T_1 to T_2) to the calibration to scanner tubes (T_3 to T_2). Switching the "calibrate-zero" switch to the zero position (with the "on-off" switch in the on position) operates the fifth pressure switch; switching from the calibration to manifold tube (T_1 to T_2) to the zero (reference pressure) to manifold tube (T_3 to T_2). Reference pressure is routed into the other four pressure switch's

T_3 tubes where it then continues through the open T_3 to T_2 passageways and on out to the four scanners. The ZOC feature is also easily programmed into a data acquisition system for on-line zeroing and calibration during actual testing. Together with the 12M Scanivalves, the ZOC feature permits gathering of more accurate pressure data than existing pressure scanning systems.

The fluctuating pressures are measured by five miniature Kulite Model XCQL-093 pressure transducers. The pressure sensing diaphragms are mounted flush with the inlet surface. An Ectron Model P516-5SG Strain Gage Power Supply is used to provide excitation voltage to the Kulite transducers. The signals from the Kulite transducers are amplified by D.C. Ectron Model 562 FJ Amplifiers and recorded on a Bell & Howell Model CPR-4010 Tape Recorder. Figure 20 presents a schematic of the fluctuating pressure measuring system. The fluctuating pressure measurement will help to identify the character of the boundary layer and location of separation regions.

IV. RESULTS AND DISCUSSION

Injector Calibration

Before installing the inlet model, the injector was tested for efficiency, maximum mass flow rate, and maximum period of constant induced mass flow rate. The piping which connects to the injector and through which the induced air travels was left open to the wind tunnel room at the flange closest to the ceiling (Fig. 3). The mass efficiency of the injector is the most important parameter in our application and it is defined as the ratio of the induced mass flow rate to the injected mass flow rate. Since the mass efficiency depends mainly on the injection pressure and injection slot area, these two parameters were treated as the independent variables. Injected mass flow rate was determined from the measured injected flow parameters and the slot area by using the assumption of choked flow in the slot. The induced mass flow rate was estimated on the basis of measurements made with a pitot-static tube installed in the injector inlet pipe. Details of mass flow rate calculations are presented in the Appendix. Values of the induced velocity were measured at different injection pressures for the range of injection slot area and are plotted in Figure 21. It can be seen that smaller injection slot areas require higher injection pressure to obtain the same induced velocity. The induced velocity reaches a maximum (corresponding to a dynamic pressure of about 84 inches of water) when the induced flow in the injector itself is choked. Increasing the injector pressure beyond the choked flow limit causes a drop in induced velocity which is believed to be caused by the increased supersonic expansion of the injected

air which effectively reduces the cross sectional area available for the induced air in the injector.

Injector mass efficiency ($\dot{m}_i/\dot{m}_j$) versus regulated injection pressure for the range of injection slot area is plotted in Figure 22 (units of $\dot{m}$ are in lb_m/sec). From this graph it can be seen that injector efficiency increases for decreasing injection slot area with maximum efficiency at the minimum injection slot area. Also, the injector efficiency is a function of regulated injection pressure. On the basis of these results it was decided to use the minimum injector slot area for testing inlet models. With such an arrangement, available run times were maximized.

During calibration testing of the injector it was observed that constant induced mass flow rate could easily be obtained for run times up to two minutes for the low induced mass flow rates. As the induced mass flow rate increased, the run time decreased.

Mass flow rates of the induced air were established on an assumption of a constant velocity profile at the measuring station of the pipe. Consequently the values of mass flow rates and injector efficiency may be in error by a few percent. It was not desired to accurately determine the injector efficiency, rather it was desired to perform comparative tests and determine which area would provide the maximum injector efficiency.

Preliminary Investigation of Inlet Models

Presented in this section are the results of six different test runs for the two inlet models. Surface static pressure distributions are used primarily to indicate separation and its location. Boundary layer rake data is used to back up several cases where there is strong evidence of separation as given by the surface static pressure distributions. Boundary layer rakes measure only the "outer most" part of the boundary layer. If the total pressures measured by a boundary layer rake do not recover in this "outer most" layer and above, and if these pressures are close to the value of the local surface static pressure, then there is a good indication that the flow has separated. Several Shadowgraph pictures are presented as further back up evidence for clearly separated cases only. As already indicated, the two investigated inlet models have essentially the same profile shape but they differ in the contraction ratio. The thicker lip inlet, designated as GE-2, has the contraction ratio of 1.46 and the thin lip inlet, GE-1, has the contraction ratio of 1.37. Figure 23 presents the windward surface static pressure distributions for the two inlets at zero incidence angle, a freestream velocity, U_∞, of 150 ft/sec, and a low mass flow rate corresponding to a throat Mach number, M_T, of 0.38. Both inlets display characteristic pressure drop in the highlight region and a subsequent pressure increase along the lip and the diffuser sections. Both inlets exhibit a small adverse pressure gradient and the flow remains well attached along the entire surface. Figure 24 shows surface static pressure distributions for the same throat Mach number but at an incidence angle,

α, of 15°. The increase in α has resulted in an increased expansion around the highlight which, in turn, has increased the adverse pressure gradient along the downstream portion of the inlet surface. The flow in the GE-2 inlet remains essentially attached except for a small separation bubble which possibly exists near the location of S/L=0.1*. The pressure distribution for the GE-1 inlet provides an indication of the boundary layer separation somewhere upstream of S/L=0.2. This is evidenced by a sharp change in slope of the rising static pressure ratio near the location of S/L=0.2. Further increase of the incidence angle to 30° (Fig. 25) has caused the flow in the GE-2 inlet to separate near a location S/L=0.15. For the GE-1 inlet, the boundary layer separation which was already present at 15° has somewhat intensified, however the initial separation point has not moved upstream as it might be expected. The pressure distribution for configuration GE-1, α=30°, exhibits a flat pressure plateau followed by an abrupt pressure increase. So far, we do not have any explanation for this type of pressure variation.

Figures 26, 27 and 30 show the pressure distributions at 0°, 15° and 30° for the case of relatively high mass flow rate corresponding to M_T=0.73. At α=0°, the flow in the GE-2 inlet expands to supersonic speeds around the entry lip and then recompresses through a shock system near S/L=0.2. There is no clear evidence of flow separation due to the shock/boundary layer interaction. The flow around the highlight of the GE-1 inlet expands to higher supersonic velocities than in the GE-2 inlet; despite this face, the subsequent recompression appears to be

*The ratio S/L is the dimensionless surface distance from the highlight.

relatively smooth and free of separation. When the angle of incidence is increased to 15°, the initial supersonic expansion in both inlets intensifies, but particularly in the GE-1 inlet, and the resulting adverse pressure gradient is evidently large enough to cause flow separation. The separation is particularly evident for the GE-1 inlet. Back-up evidence is provided by pressure data from boundary layer rake #2 (S/L=0.65). Figure 28 is a plot of this data which compares the two inlet models. The GE-1 inlet has a constant P_R/P_o value of about 0.7 which agrees with P/P_o from the surface static pressure distribution at S/L=0.65 (Fig. 27). Since the total pressure does not recover as the distance from the surface increases vertically, separation is strongly indicated. The GE-2 inlet may not be as strongly separated as the GE-1 inlet. Figure 29 is a Shadowgraph picture of inlet model GE-1, and is presented as back-up evidence of flow separation for the conditions of Figure 27. Further increase in the incidence angle to 30° moves the separation point upstream toward the highlight. While this upstream motion is only slight for the GE-2 inlet, it is very pronounced for the GE-1 inlet, where the flow separates very near the highlight exhibiting the case of the so called lip separation. This type of flow separation is known to have a very detrimental effect on the fan and engine operation. Figure 31 is a plot of boundary layer rake #1 (S/L=0.27) for this case. Notice that the GE-1 inlet is separated at this point as seen by the constant P_R/P_o value of about 0.6. This value of P_R/P_o agrees with the value of P/P_o at S/L=0.27 in Figure 30. Inlet GE-2 may not be separated as strongly. Figure 32 is a plot of boundary layer rake #2 (S/L=0.65) for this same case. Both inlets are exibiting roughly the

same constant P_R/P_o value which agrees with the value of P/P_o from Figure 30 at S/L=0.65. This data tends to back up the results from the surface static pressure distribution, i.e., the GE-1 inlet separates closer to the highlight than the GE-2 inlet. Figure 33 presents a Shadowgraph picture of inlet model GE-2 for the conditions of Figure 30. Unfortunately, a photograph of inlet model GE-1, for this case, is not available for comparison of the location of separation.

Preliminary examination of the data obtained from the Kulite pressure transducers indicated that the boundary layer was turbulent for most of the test runs from the first Kulite transducer on. Boundary layer trips were installed close to the highlight in an attempt to trip the boundary layer from laminar to turbulent flow. Comparison of this data would then allow a determination of laminar or turbulent flow separation. This attempt was unsuccessfull and caused the boundary layer to separate instead of transition. From the preliminary testing, it was concluded that in most of the tests the boundary layer in the region of the separation was turbulent.

Examination of the preliminary results obtained with the two inlets indicates that, in general, an increase in the contraction ratio results in a delayed boundary layer separation. The low contraction ratio inlet (GE-1) was subject to lip separation at an incidence angle of 30° for the throat Mach number of 0.73. For the conditions of these experiments, an increase in the throat Mach number (and, thus, in the mass flow rate through the inlet) from 0.38 to 0.73 has caused

a reduction of the separation angle, i.e., the angle corresponding to an onset of flow separation.

V. CONCLUSIONS

From the results presented, several conclusions about injector performance as well as inlet flow separation at high incidence angles can be asserted.

First, the injector was found to have performance suitable for driving the air through the inlet models for incidence angles up to 60° and throat Mach mumbers up to the choked flow limit. Maximum injector mass efficiency ($\dot{m}_i/\dot{m}_j$) was established to be at the minimum injection slot area. The injection pressure control system was capable of inducing constant (within 3%) mass flow rate through the inlet model and long run times (20 to 40 seconds) for low to moderate inlet model throut Mach numbers. High inlet model throat Mach number runs were shorter, sometimes requiring manual adjustments of the injector control system during the run to maintain constant mass flow rate.

Second, inlet flow separation, in general, is delayed (α_s is increased) by an increase in the contraction ratio (thicker lip). For the conditions of these experiments, increasing the inlet model throat Mach number from 0.38 to 0.73 reduces the angle corresponding to an onset of flow separation (α_s).

REFERENCES

1. Albers, J. A., "Predicted Upwash Angles at Engine Inlets for STOL Aircraft", NASA TMX-2593, 1972.

2. Wesoley, H. L., Abbott, J. M., Albers, J. A., and Dietrich, D. A., "Low Speed Wind Tunnel Tests of a 50.8 Centimeter (20 Inch) 1.15 Pressure Ratio Fan Engine Model", NASA TMX-3062, June 1974.

3. Jakubouski, A. K., Luidens, R. W., "Internal Cowl Separation at High Incidence Angles", AIAA Paper No. 75-64, AIAA 13th Aerospace Sciences Meeting, January 1975.

4. Chou, D. C., Luidens, R. W., and Stockman, N. O., "Prediction of Boundary-Layer Flow Separation in V/STOL Engine Inlets", Journal of Aircraft, Volume 15, Number 8, August 1978.

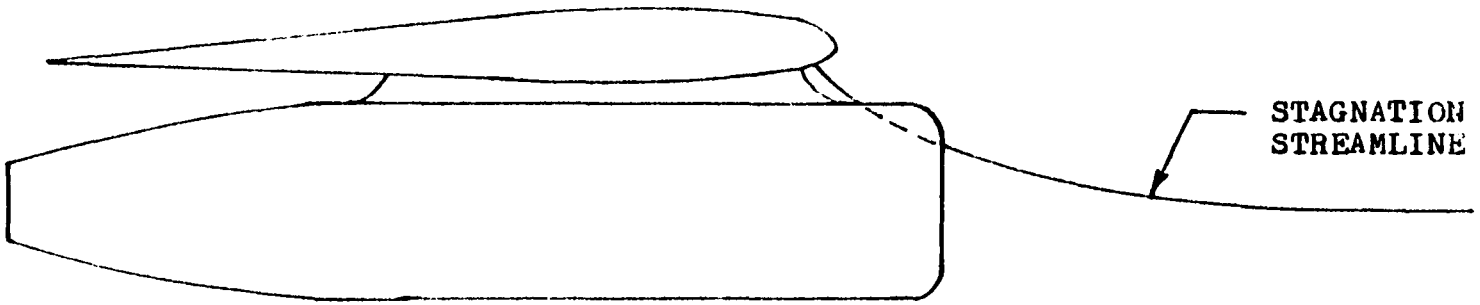

Fig. 1 STAGNATION STREAMLINE APPROACHING ENGINE UNDER WING CONFIGURATION

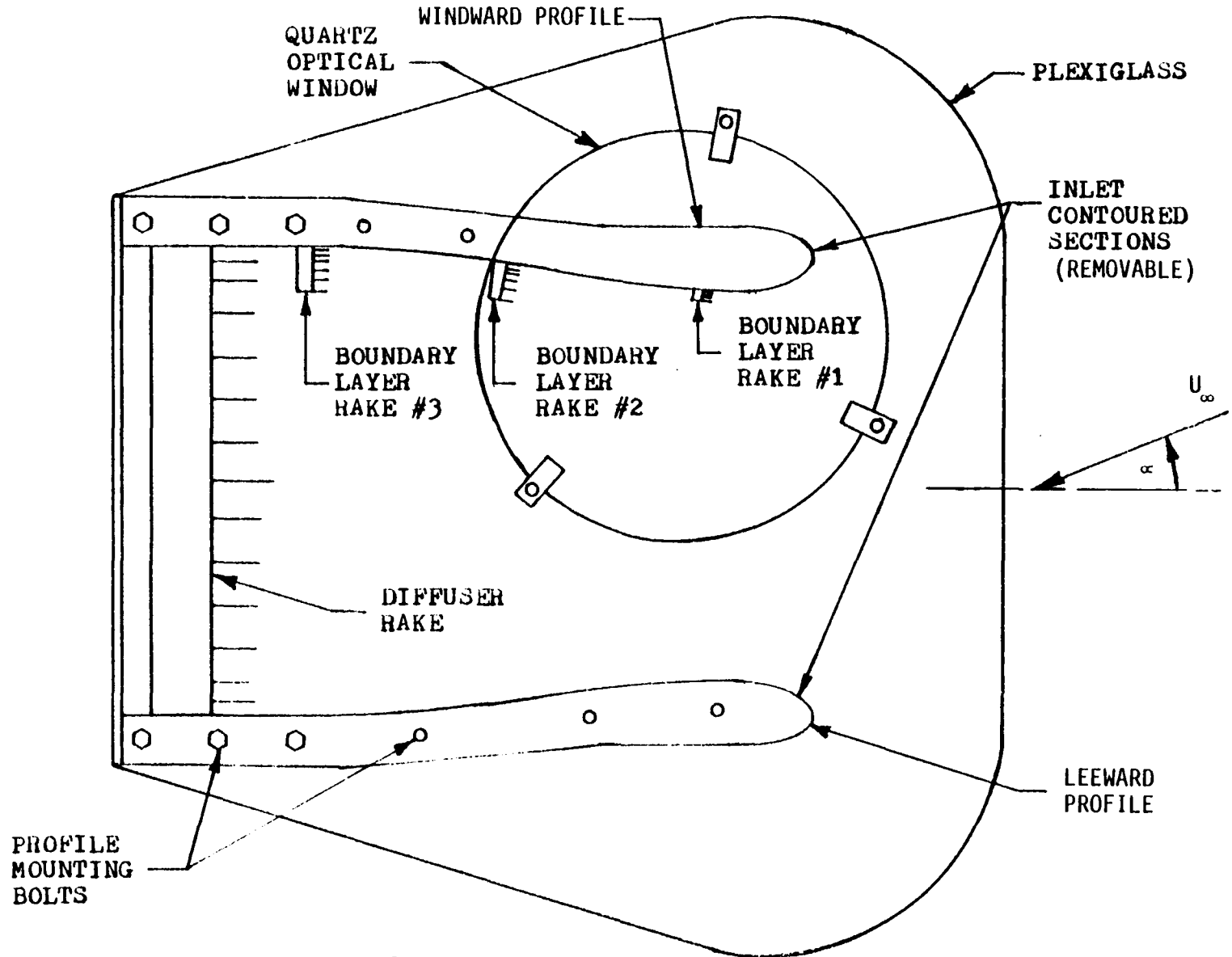

Fig. 2 SCHEMATIC OF INLET MODEL

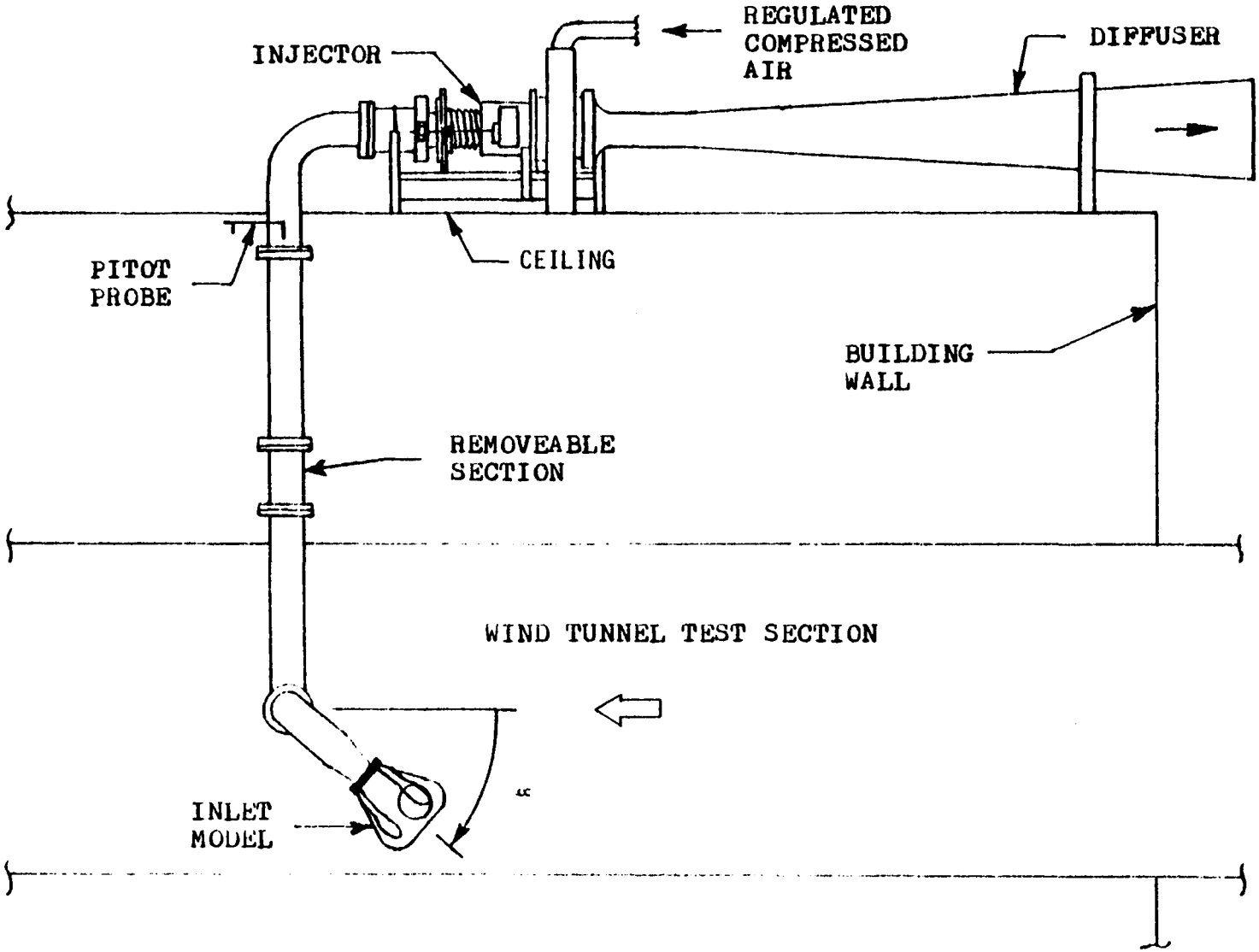

Fig. 3 FLOW INDUCTION SYSTEM

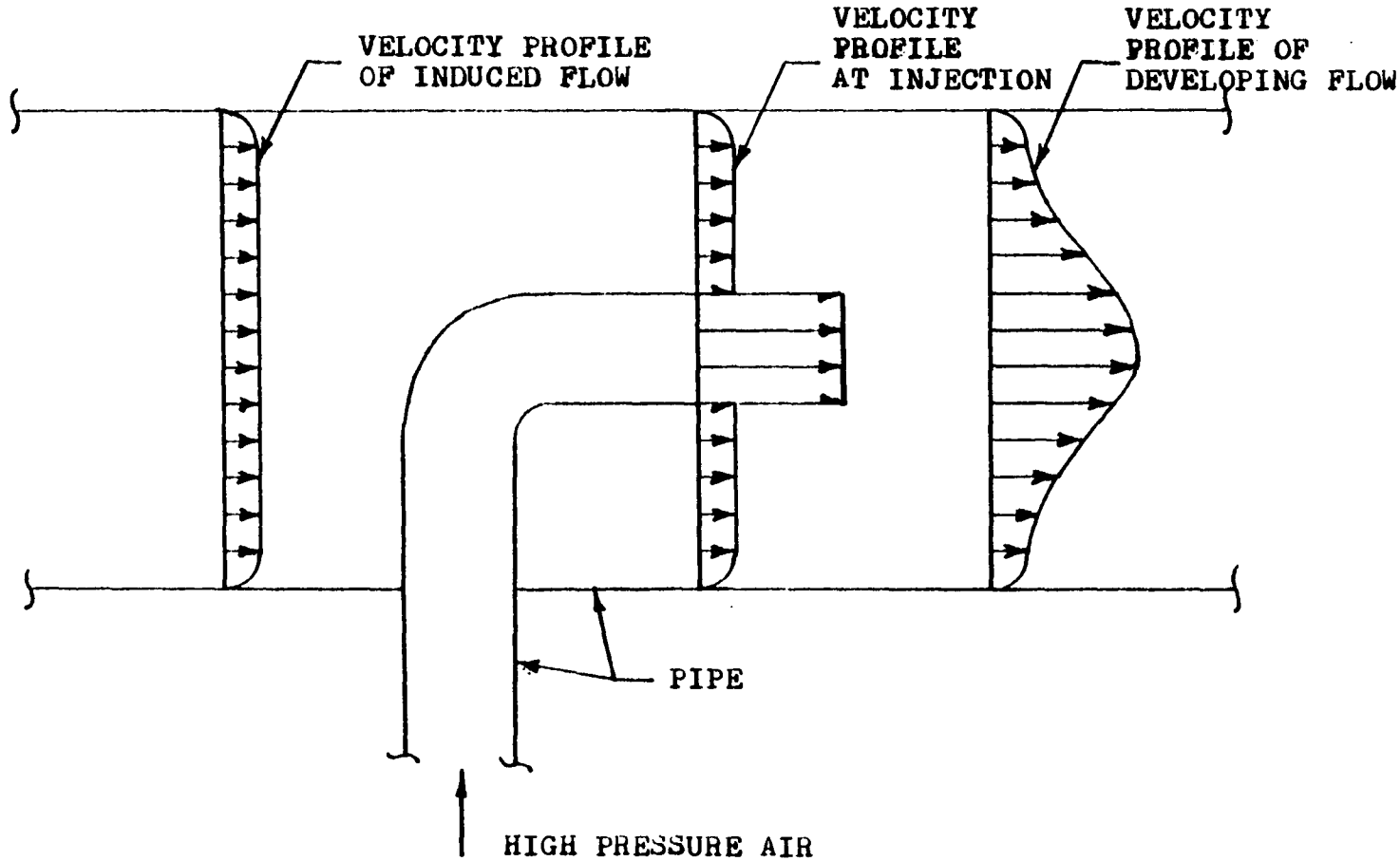

Fig. 4 SCHEMATIC OF SIMPLE INJECTOR

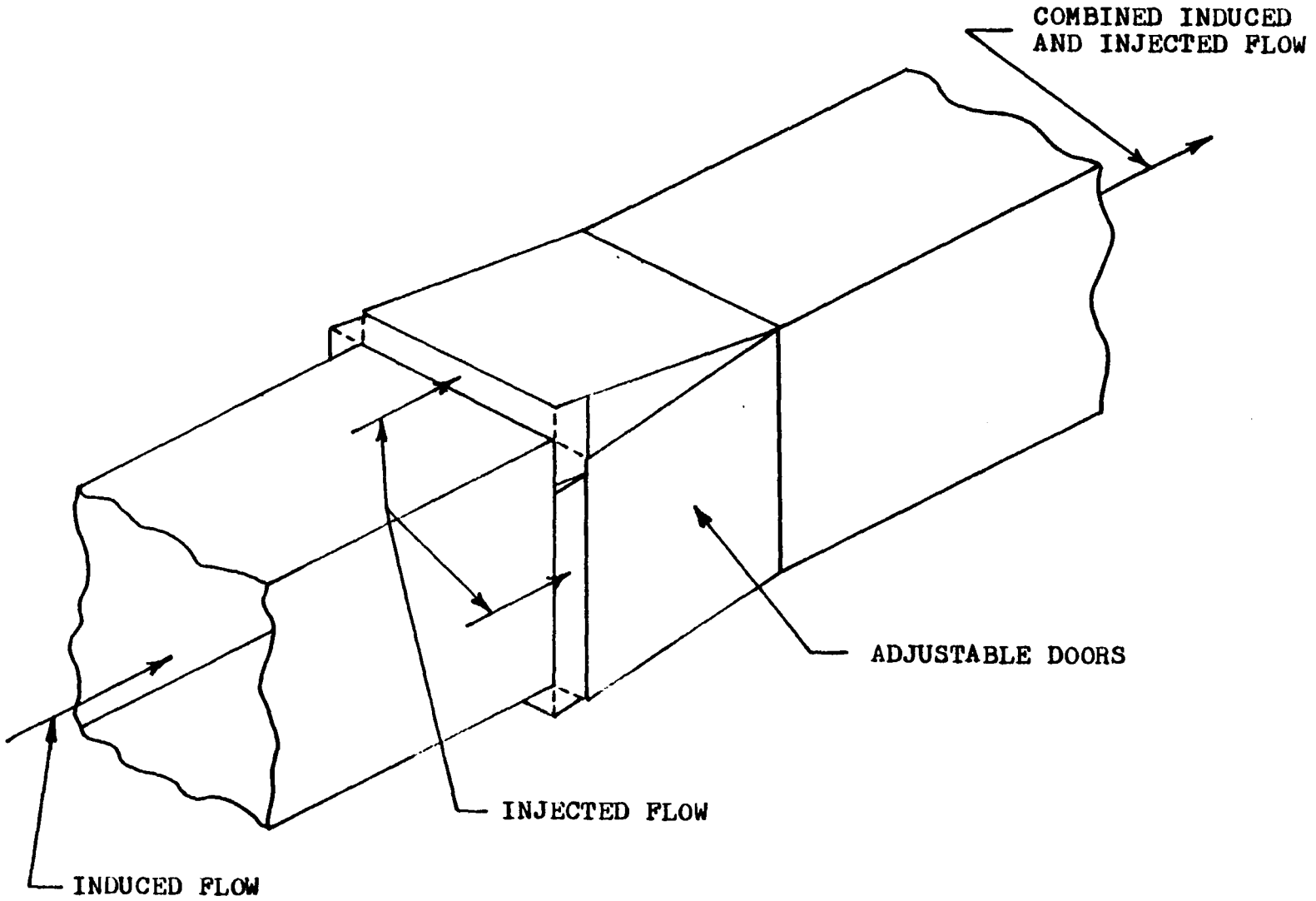

Fig. 5 SQUARE INJECTION

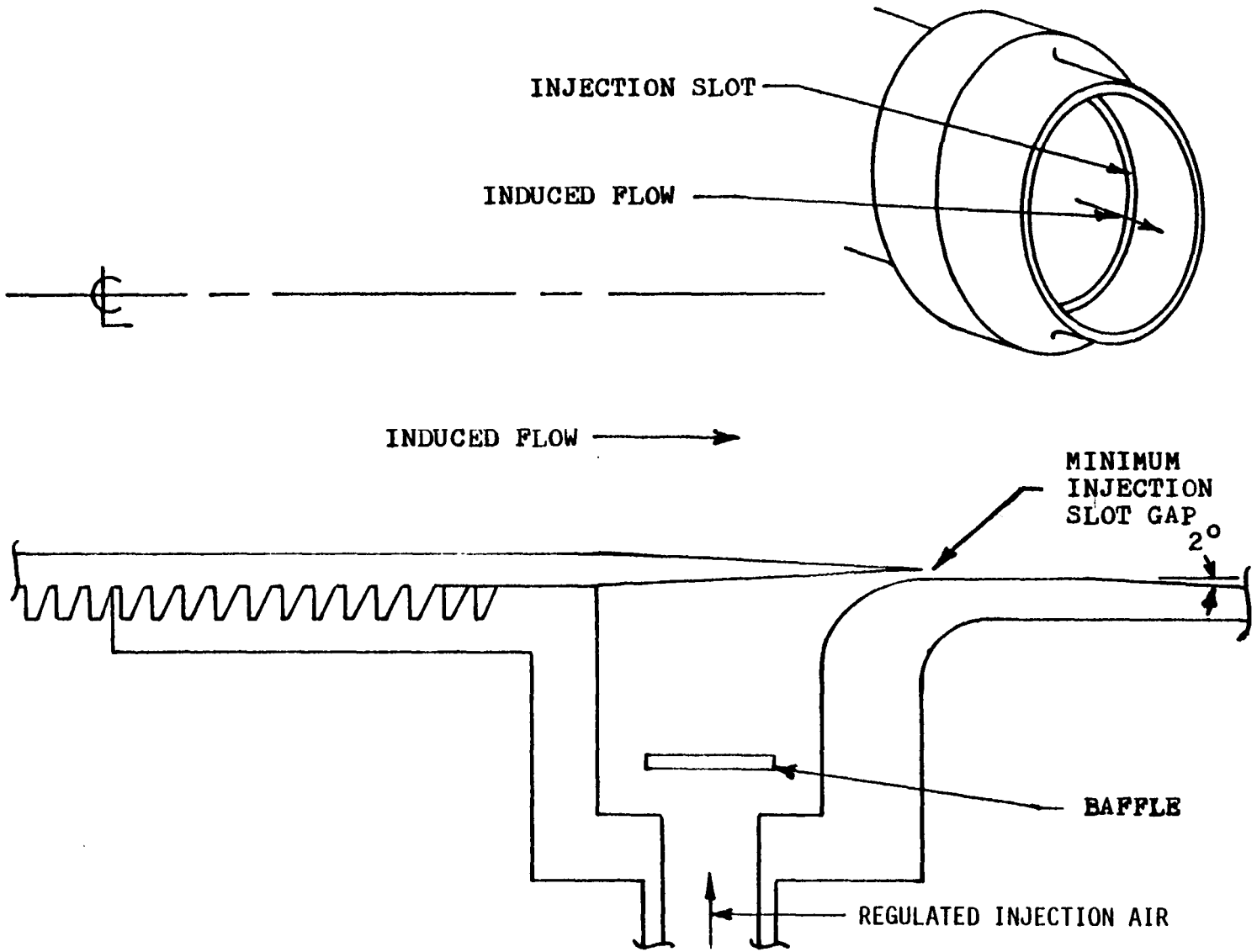

Fig. 6 CIRCUMFERENTIAL INJECTOR

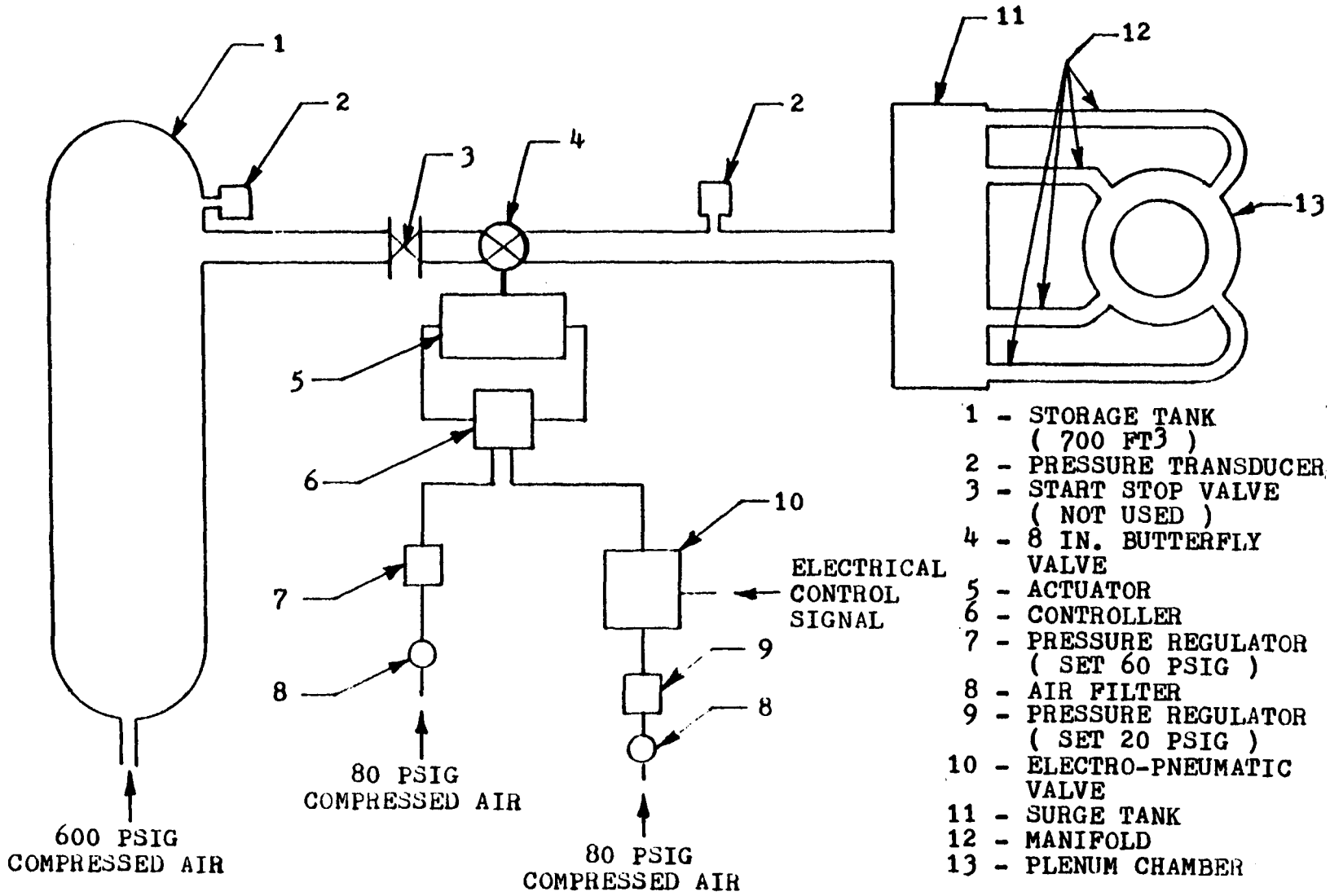

Fig. 7 SCHEMATIC OF INJECTOR PRESSURE SYSTEM AND PNEUMATIC CONTROL

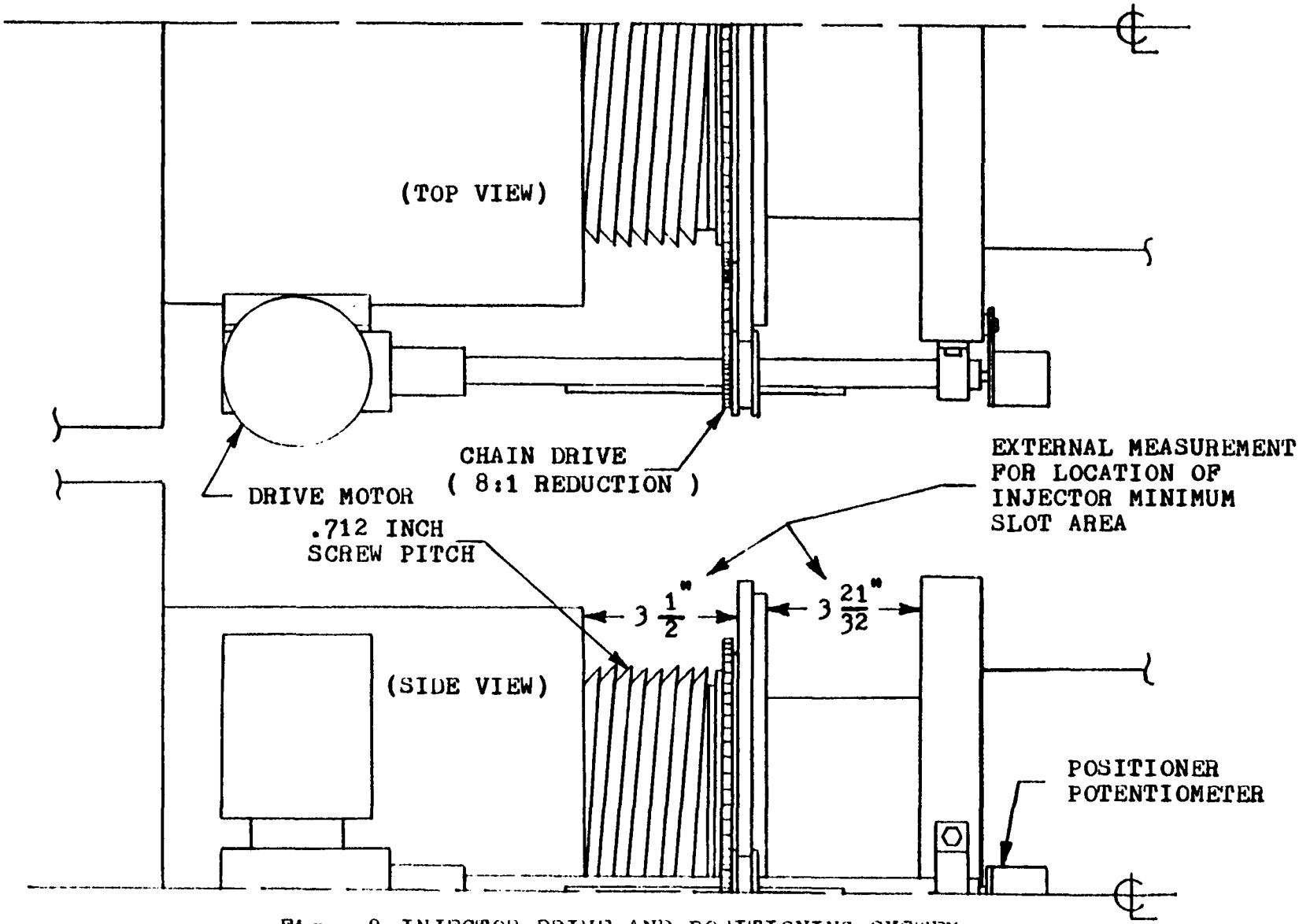

Fig. 8 INJECTOR DRIVE AND POSITIONING SYSTEM

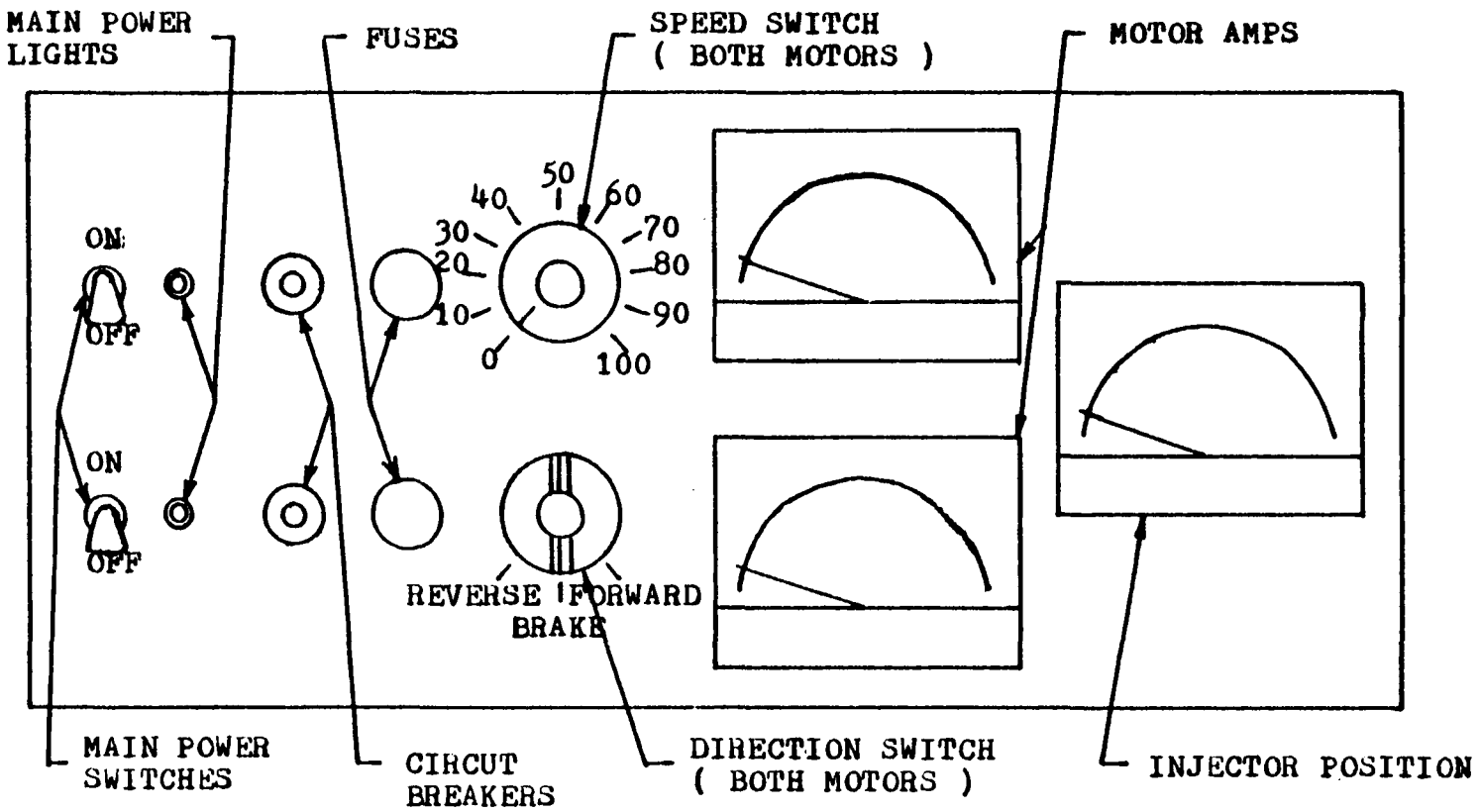

Fig. 9 INJECTOR POSITION CONTROL PANEL

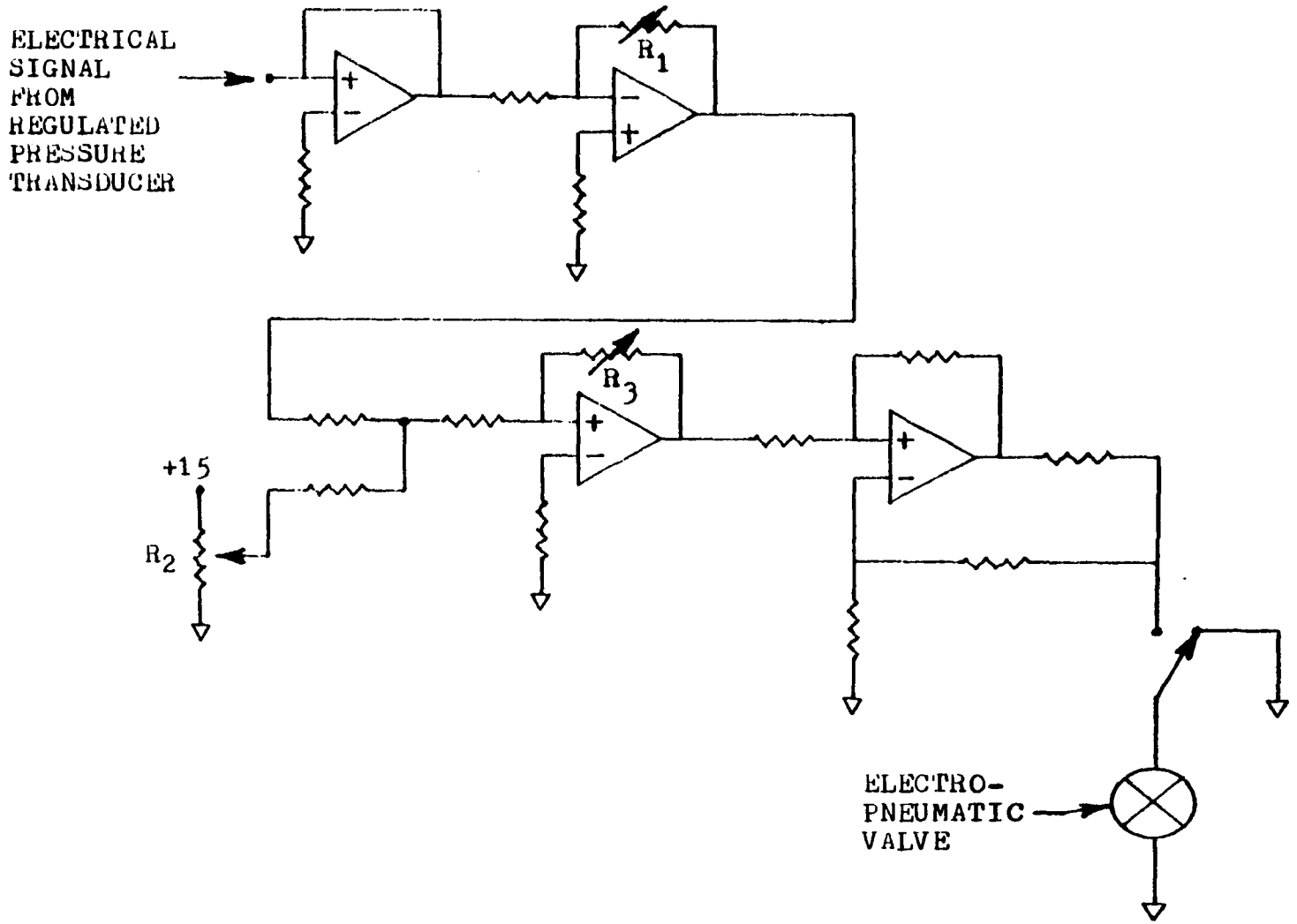

Fig. 10 CONTROL VALVE ELECTRONIC CONTROL SYSTEM
(FIRST ORDER FEEDBACK TYPE)

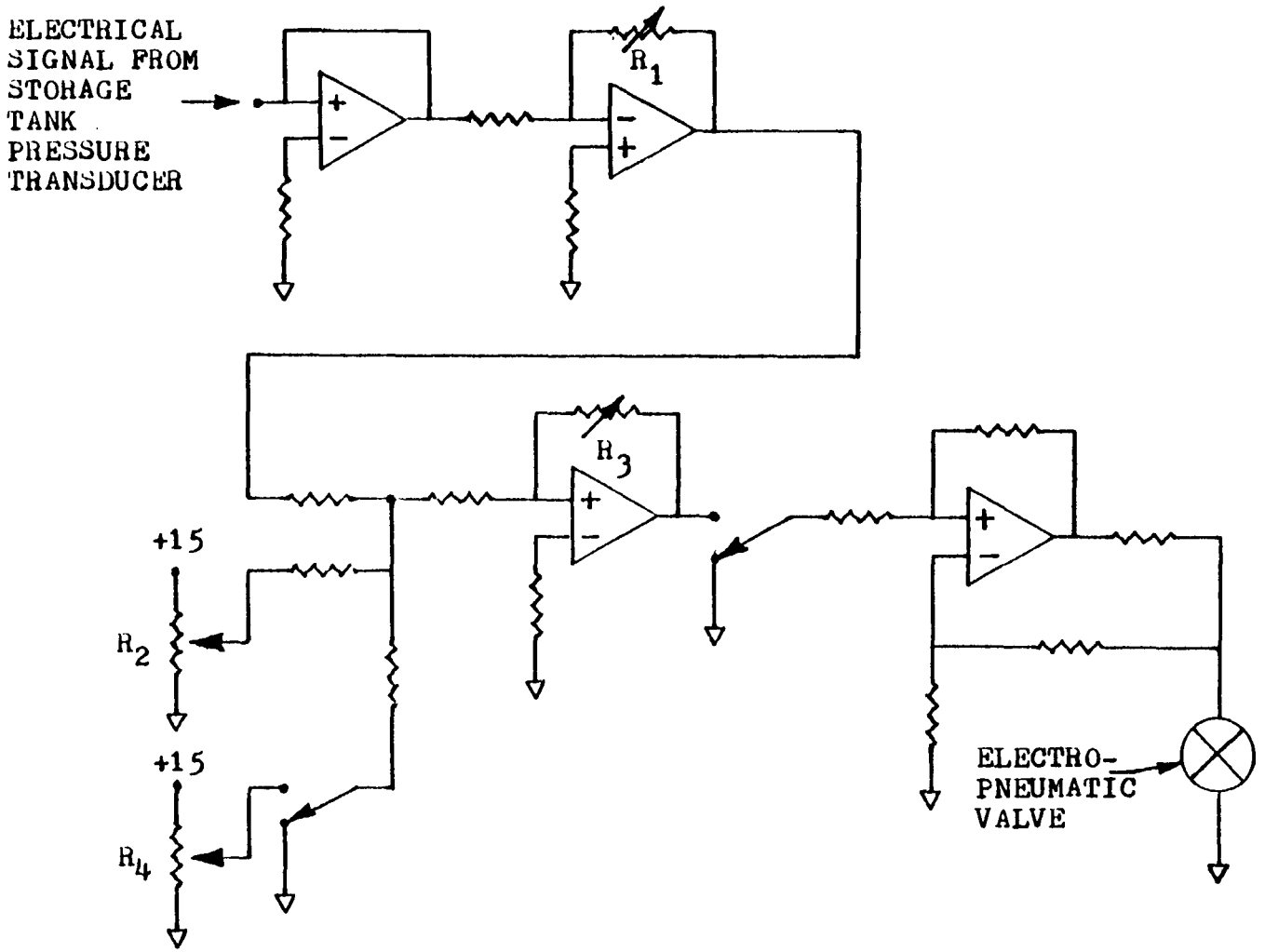

Fig. 11 CONTROL VALVE ELECTRONIC CONTROL SYSTEM
(RAMP FUNCTION TYPE)

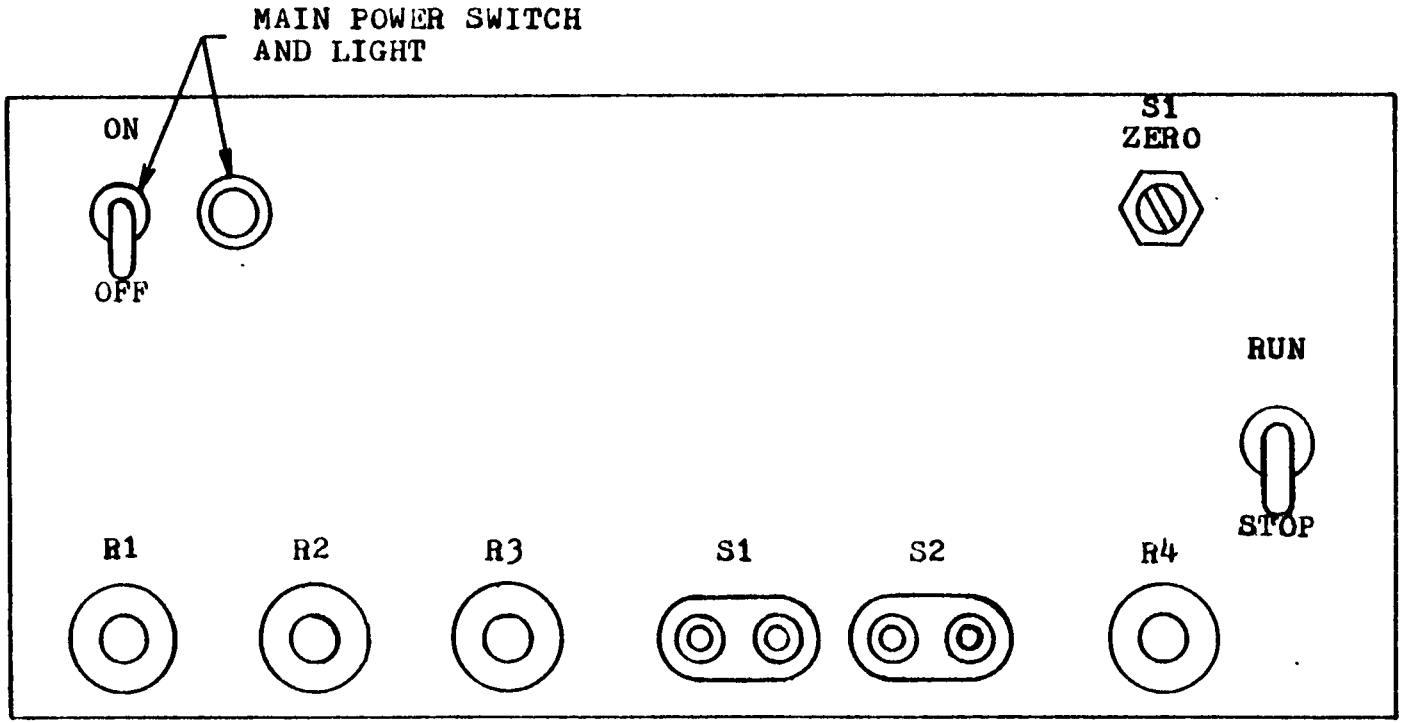

Fig. 12 INJECTOR PRESSURE REGULATION CONTROL PANEL

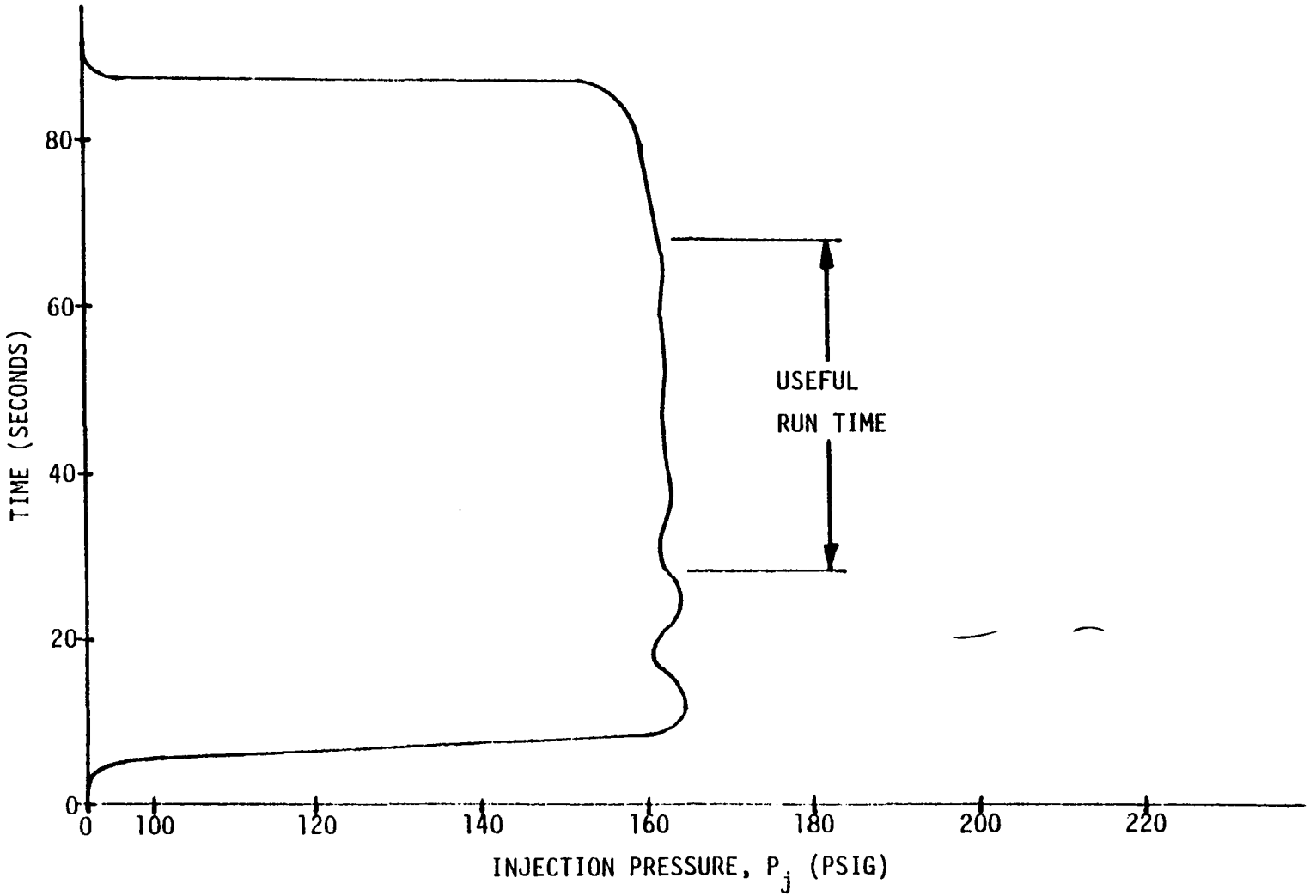

Fig. 13 TYPICAL PLOT OF INJECTION PRESSURE VS TIME FOR A LOW TO MEDIUM INLET MODEL MASS FLOW RATE

INLET MODEL	$C_r = (D_h/D_T)^2$	INTERNAL LIP CONTOUR	D_h/D_{max}	EXTERNAL FOREBODY CONTOUR	DIFFUSER ANGLE β, DEG	
					$\beta_{EQ.\ CONE}$	β_{MAX}
GE-2	1.46	2:1 ELLIPSE	.905	DAC-1	2.9	8.7
GE-1	1.37	2:1 ELLIPSE	.905	DAC-1	2.9	8.7

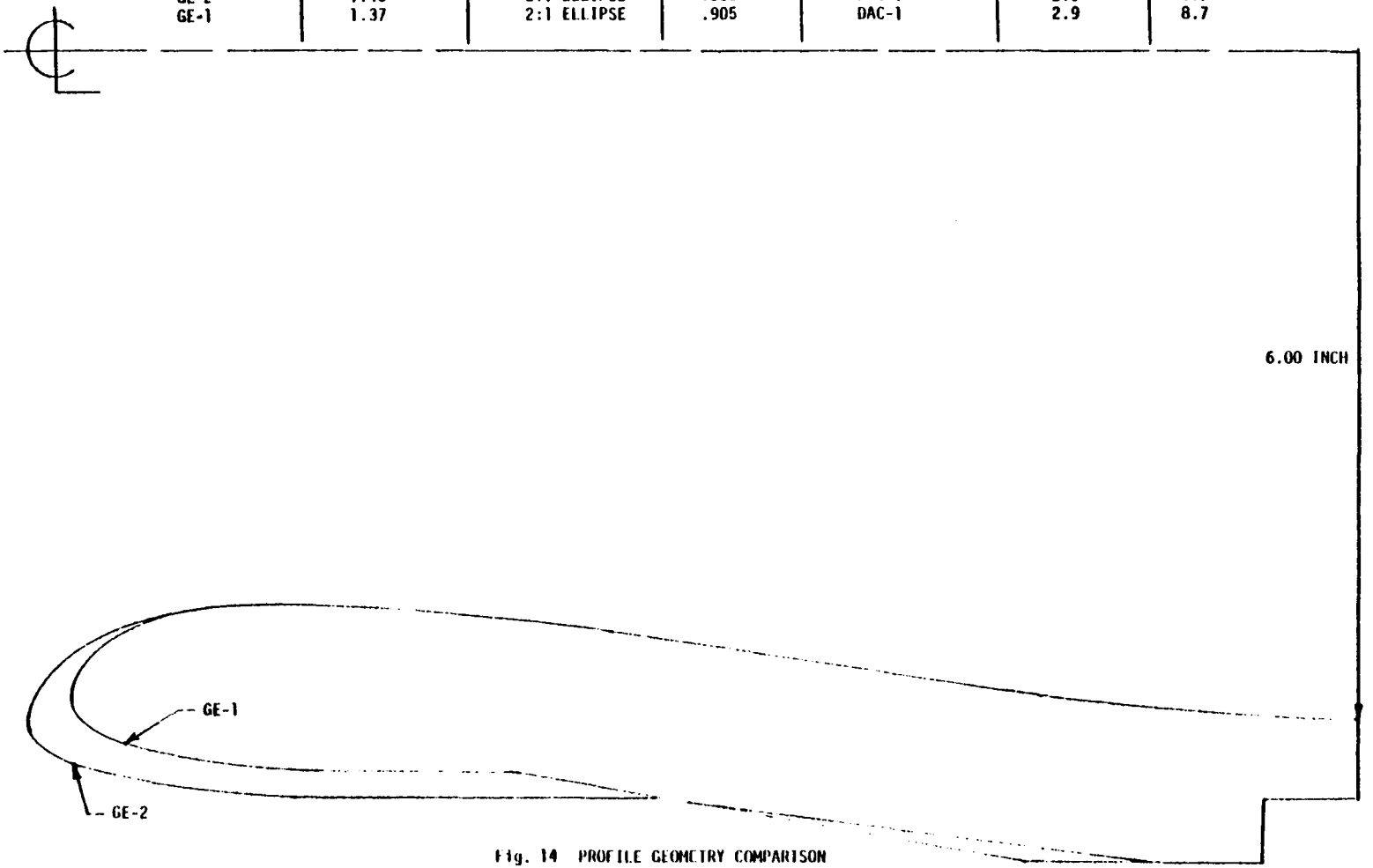

Fig. 14 PROFILE GEOMETRY COMPARISON

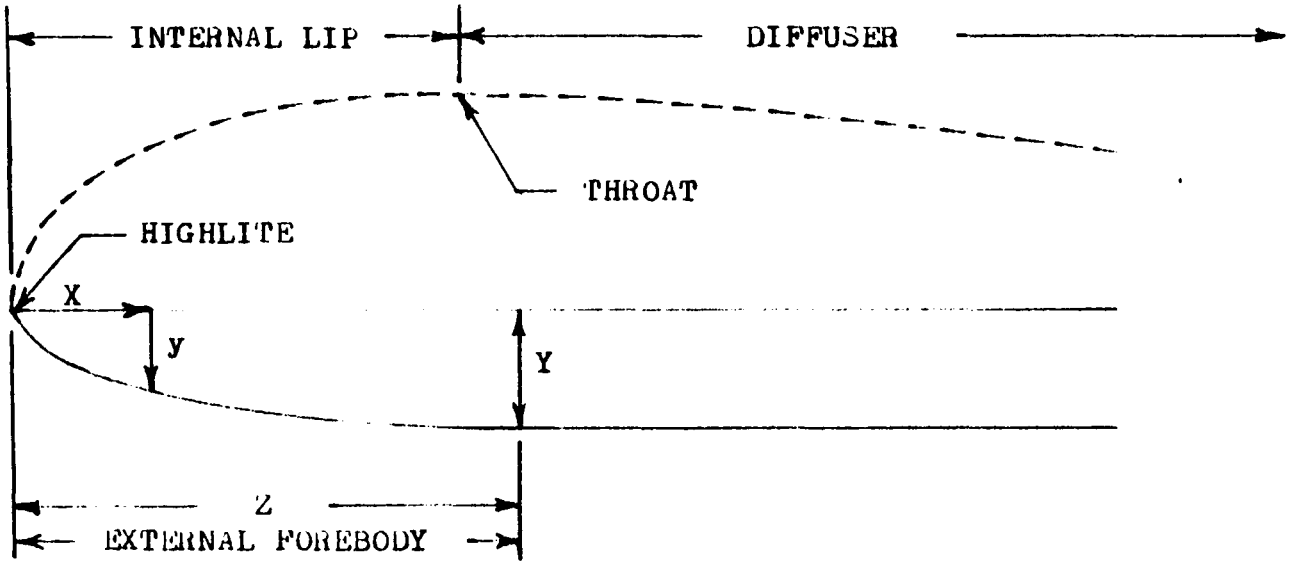

$$\left(\frac{y}{Y}\right)^2 = 2.318\left(\frac{X}{Z}\right) - 2.748\left(\frac{X}{Z}\right)^2 + 2.544\left(\frac{X}{Z}\right)^3 - 1.113\left(\frac{X}{Z}\right)^4$$

MODEL #1	MODEL #2
GE - 2	GE - 1
DAC - 1	DAC - 1
C_r = 1.46	C_r = 1.37
Y^r = .634	Y^r = .613
Z = 2.669	Z = 2.582

Fig. 15 EXTERNAL FOREBODY EQUATION

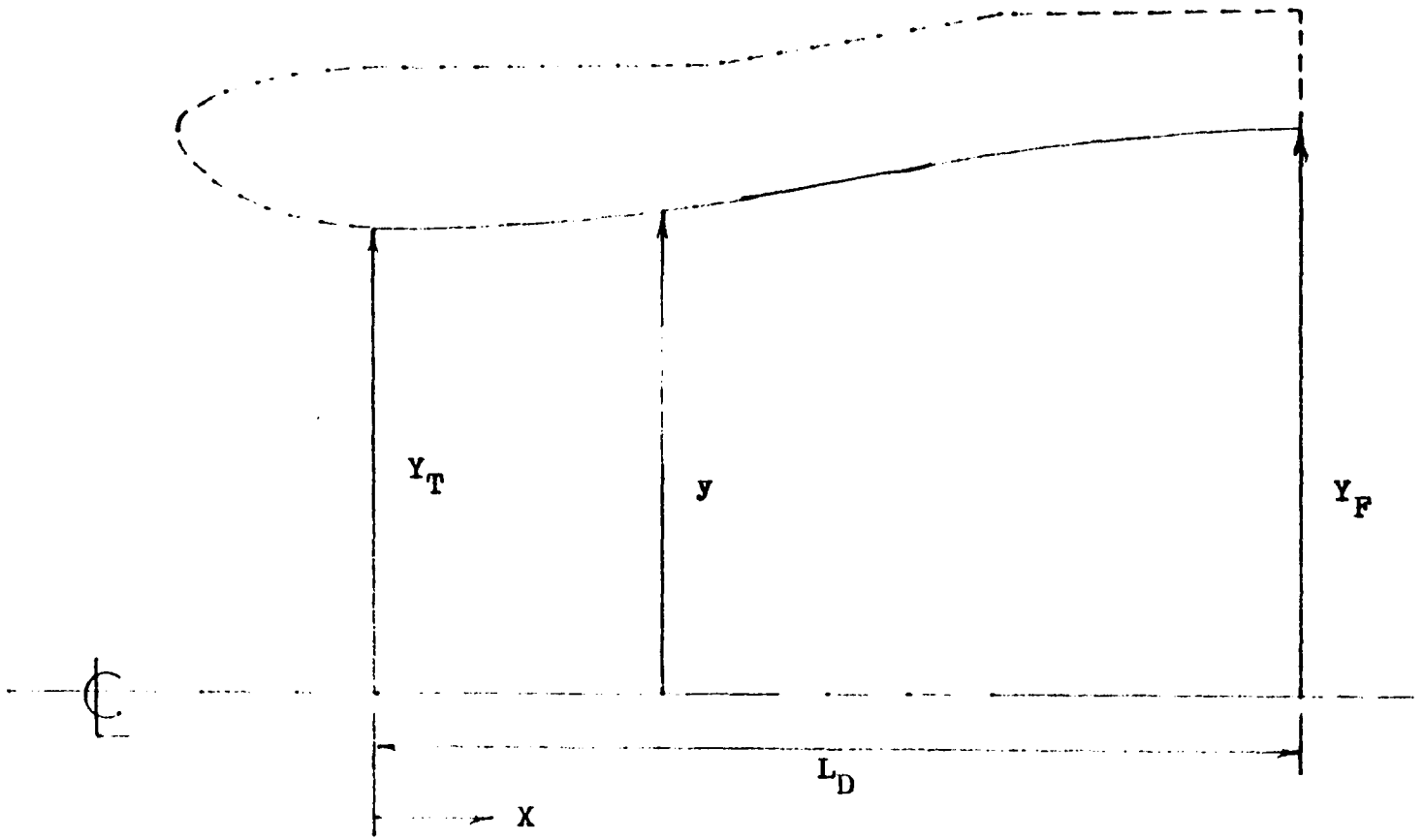

$$y = Y_T + 3(Y_F - Y_T)\left(\frac{X}{L_D}\right)^2 - 2(Y_F - Y_T)\left(\frac{X}{L_D}\right)^3$$

$Y_T = 4.991$
$Y_F = 6.00$
$L_D = 9.913$

Fig. 16 DIFFUSER EQUATION

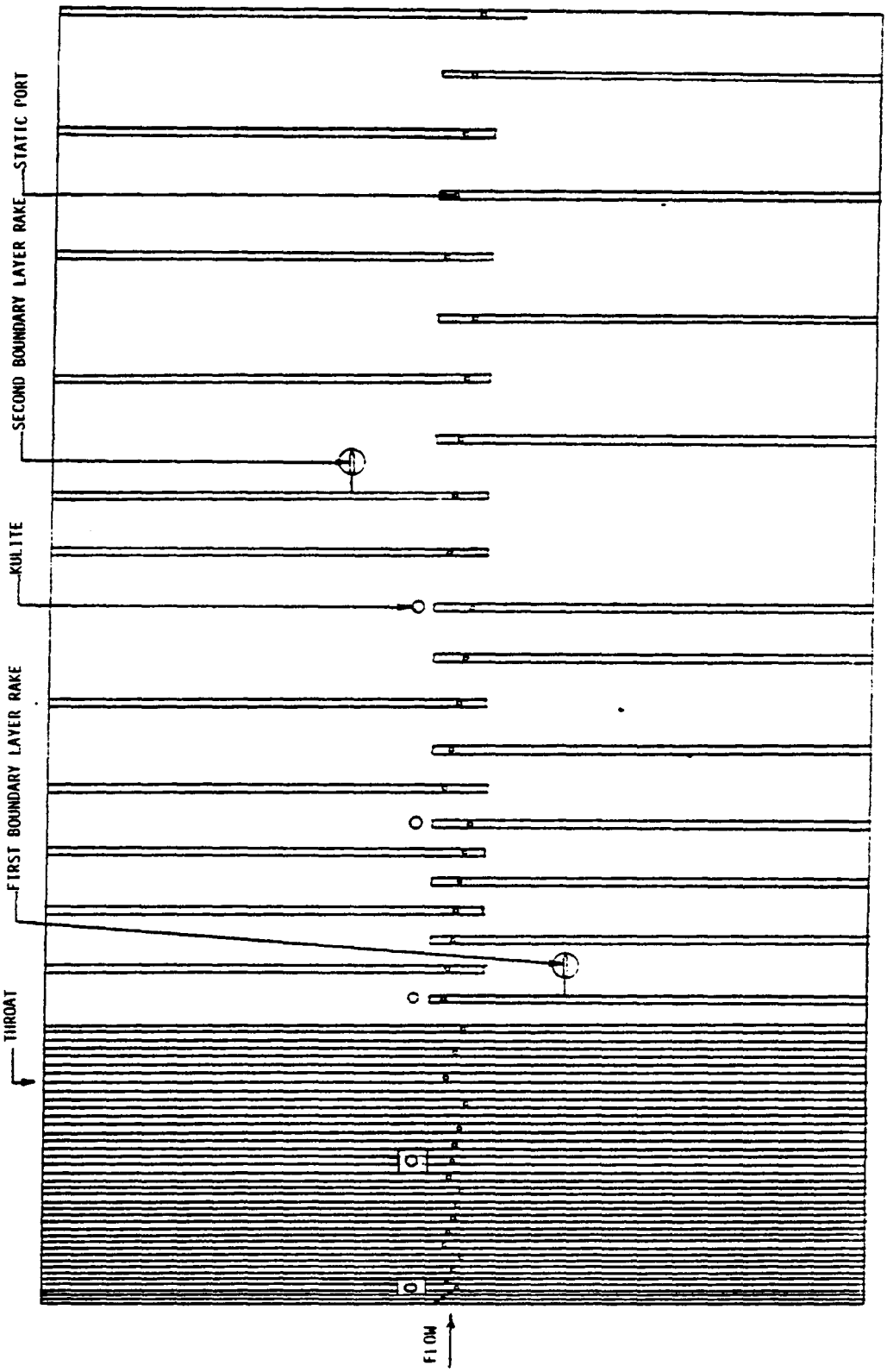

Fig. 17 PROFILE INSTRUMENTATION

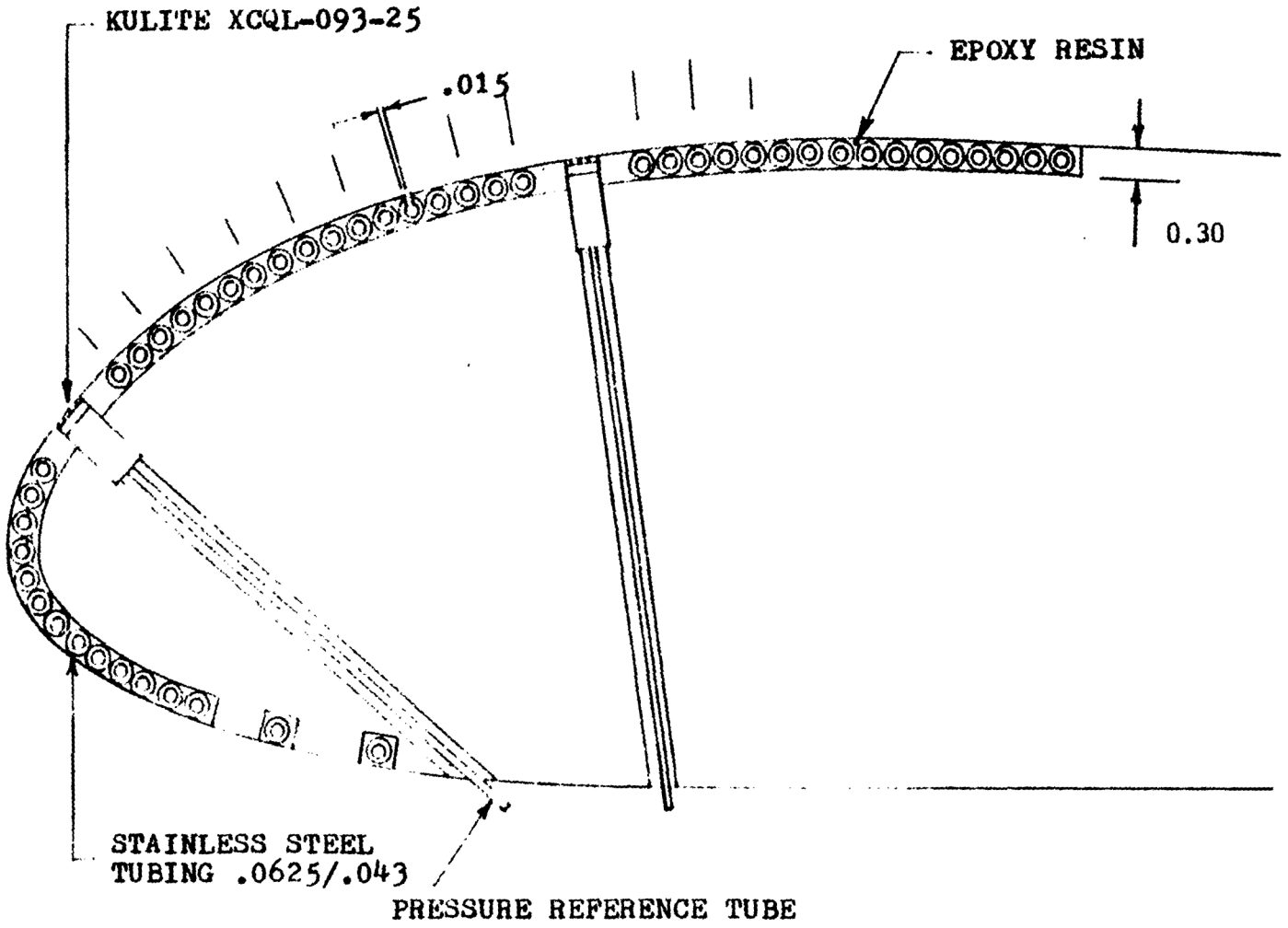

Fig. 18 DETAIL OF STATIC PRESSURE PORT MEASURING TECHNIQUE

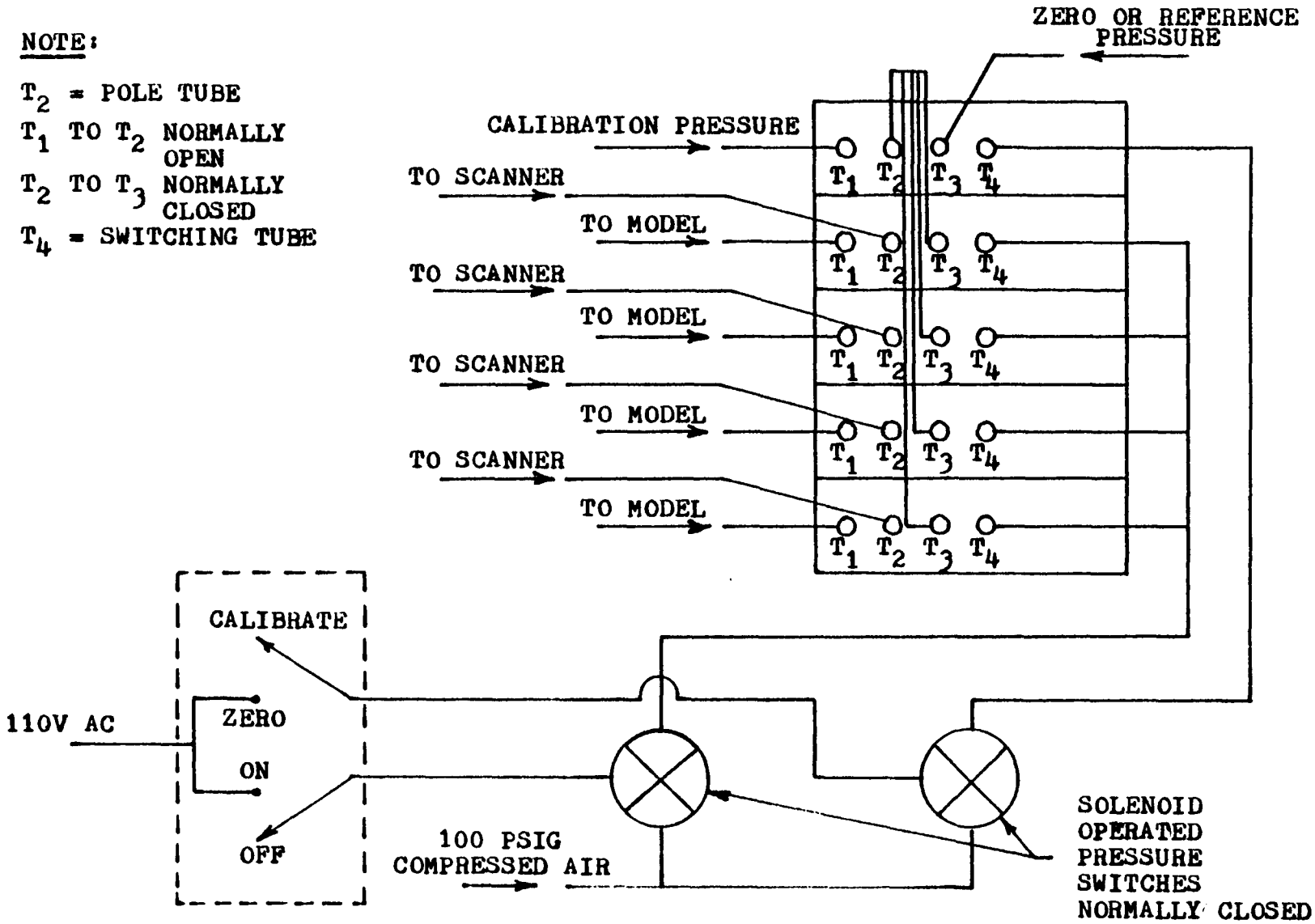

Fig. 19 ZOC SCHEMATIC

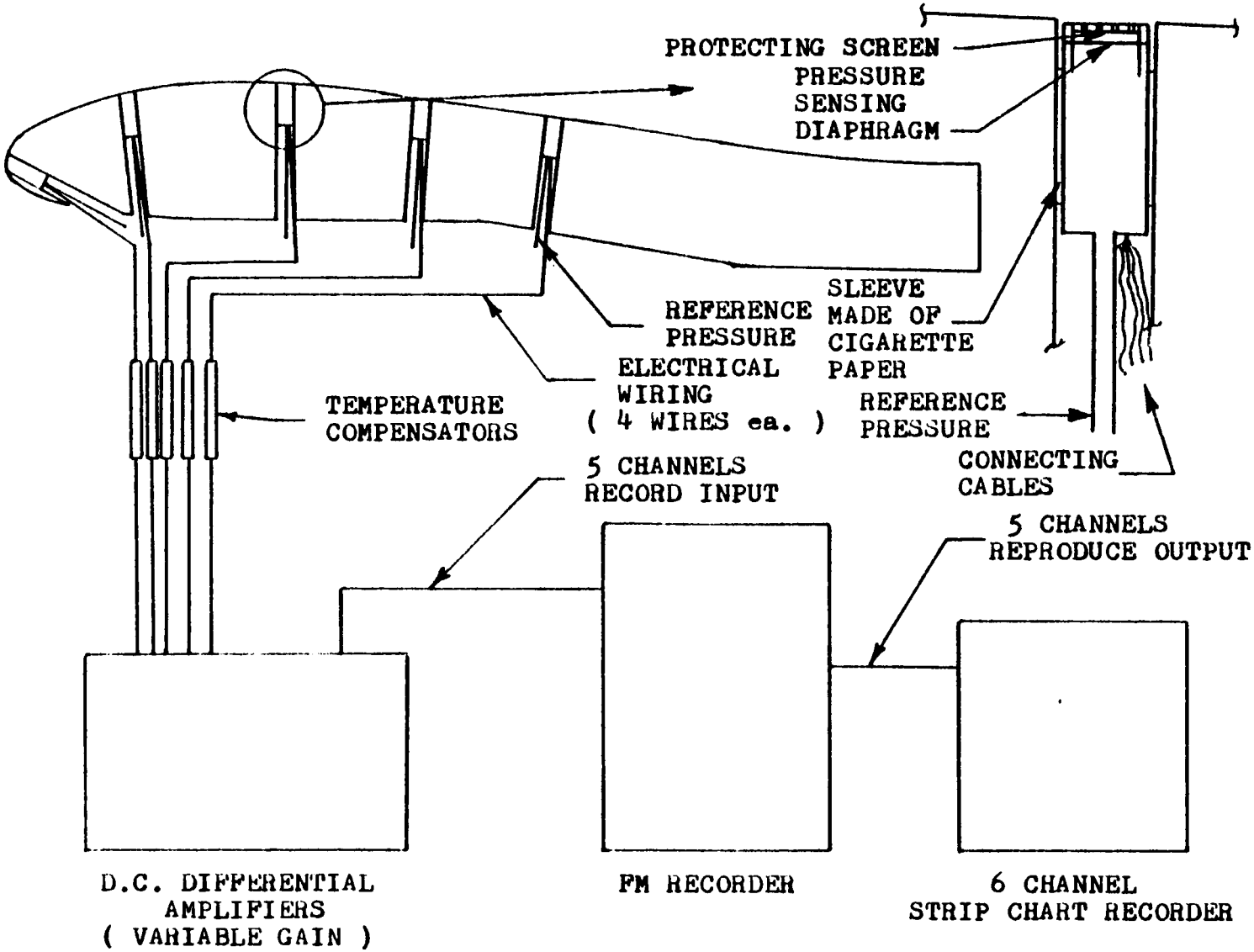

Fig. 20 SCHEMATIC OF FLUCTUATING PRESSURE MEASURING SYSTEM

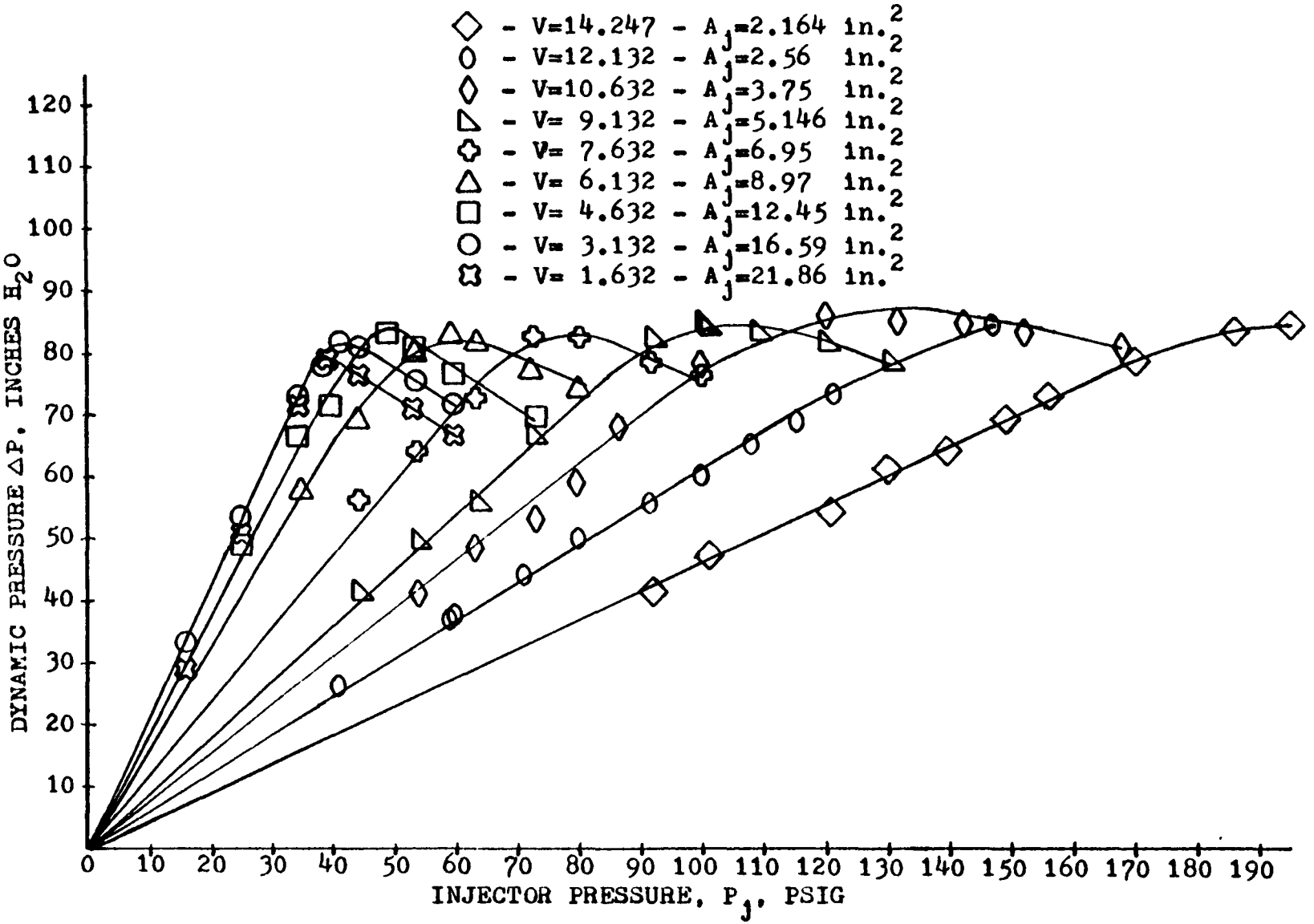

Fig. 21 DYNAMIC PRESSURE IN INLET PIPE VS INJECTION PRESSURE

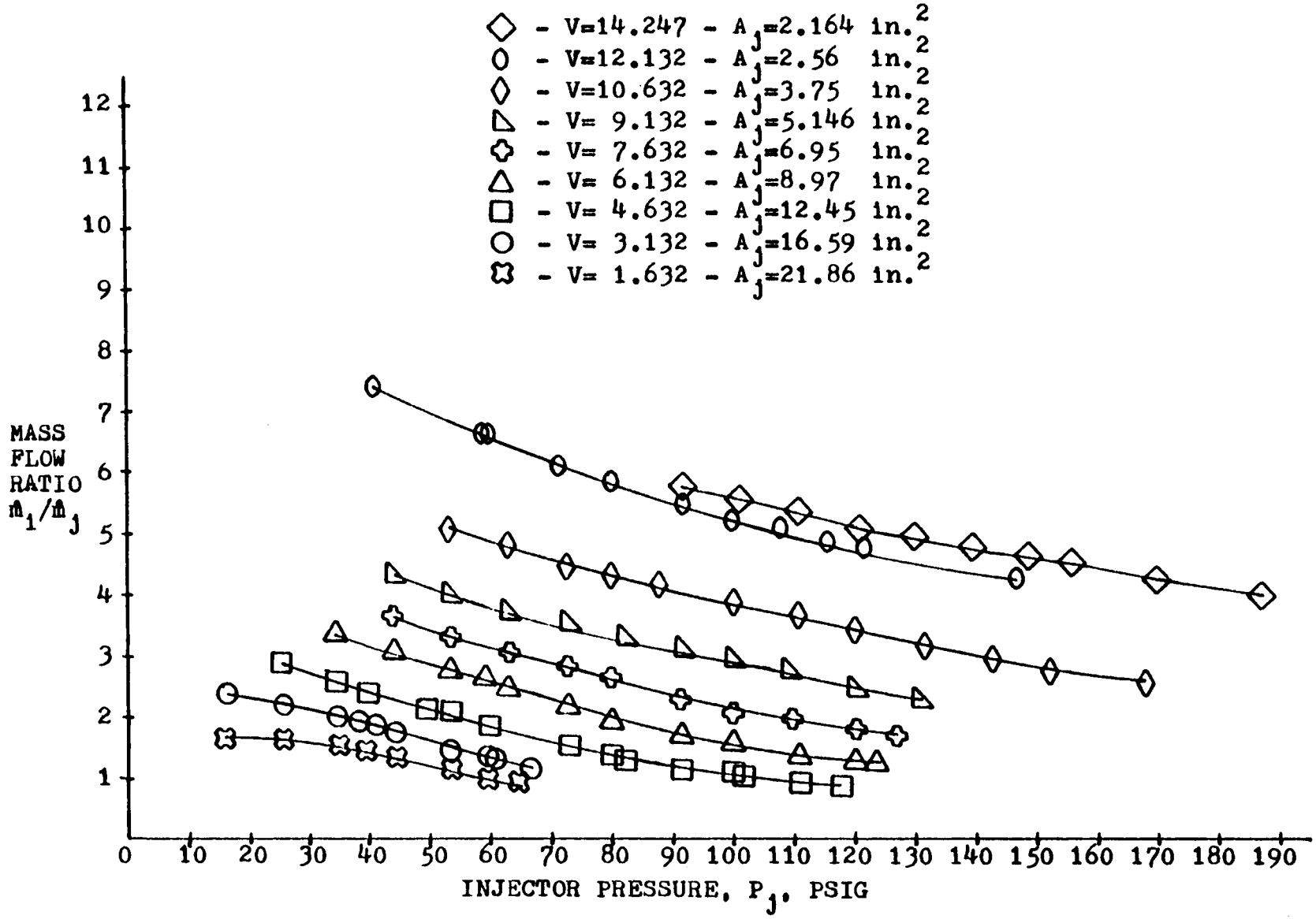

Fig. 22 MASS FLOW RATIO VS INJECTOR PRESSURE

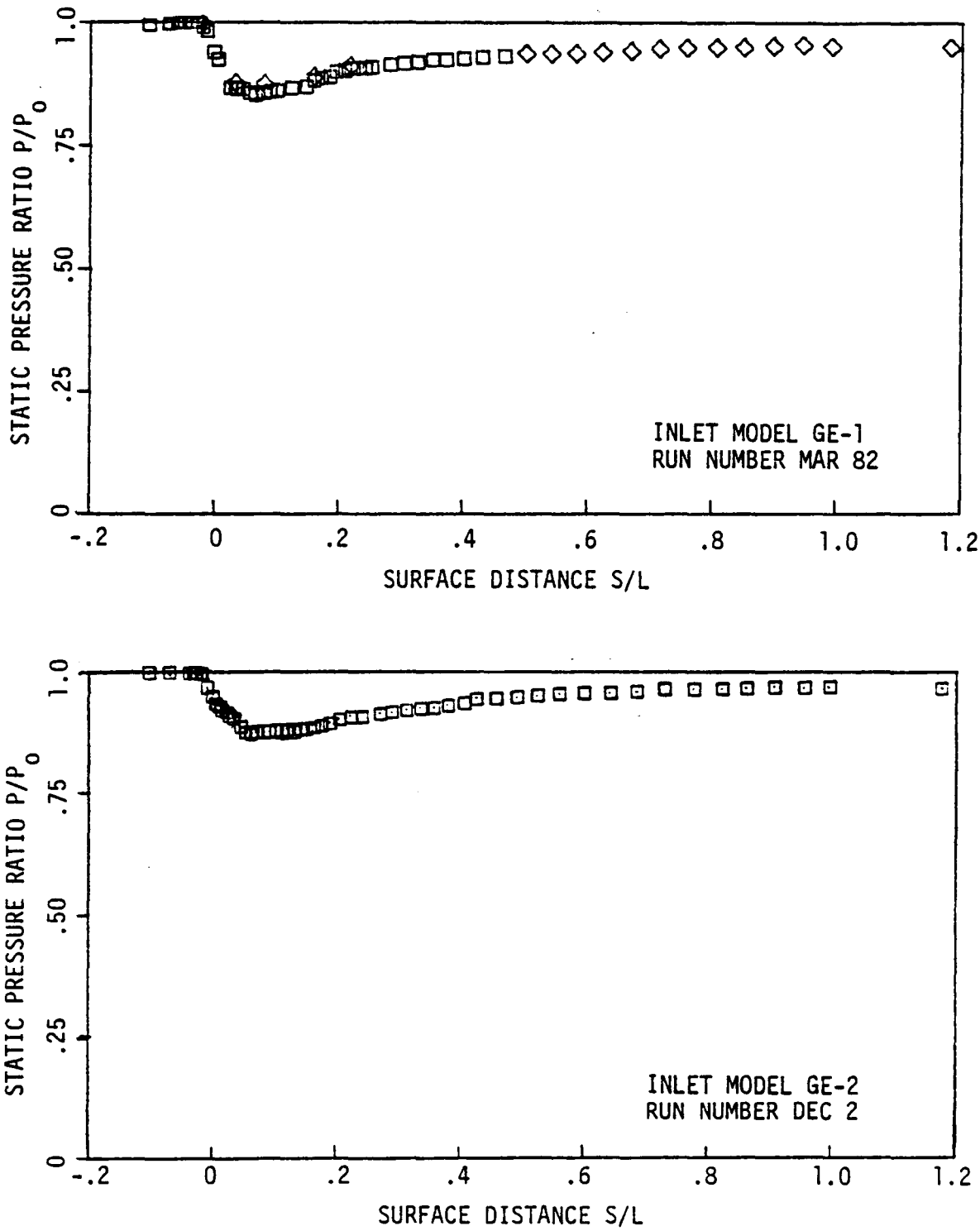

Fig. 23 INLET MODEL WINDWARD SURFACE STATIC PRESSURE DISTRIBUTION:
U_∞=150 ft/sec, M_T=0.38, α=0°

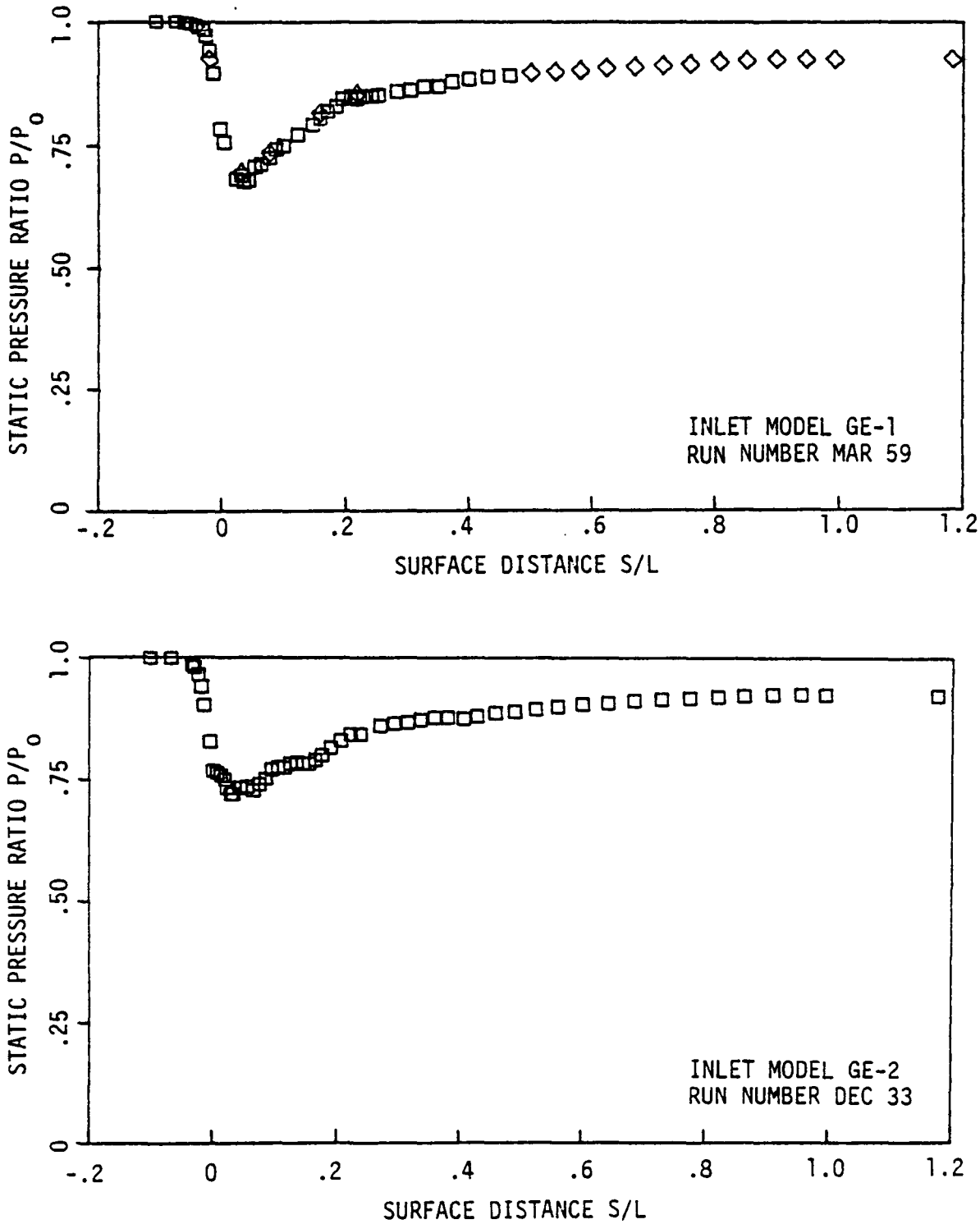

Fig. 24 INLET MODEL WINDWARD SURFACE STATIC PRESSURE DISTRIBUTION: U_∞=150 ft/sec, M_T=0.38, α=15°

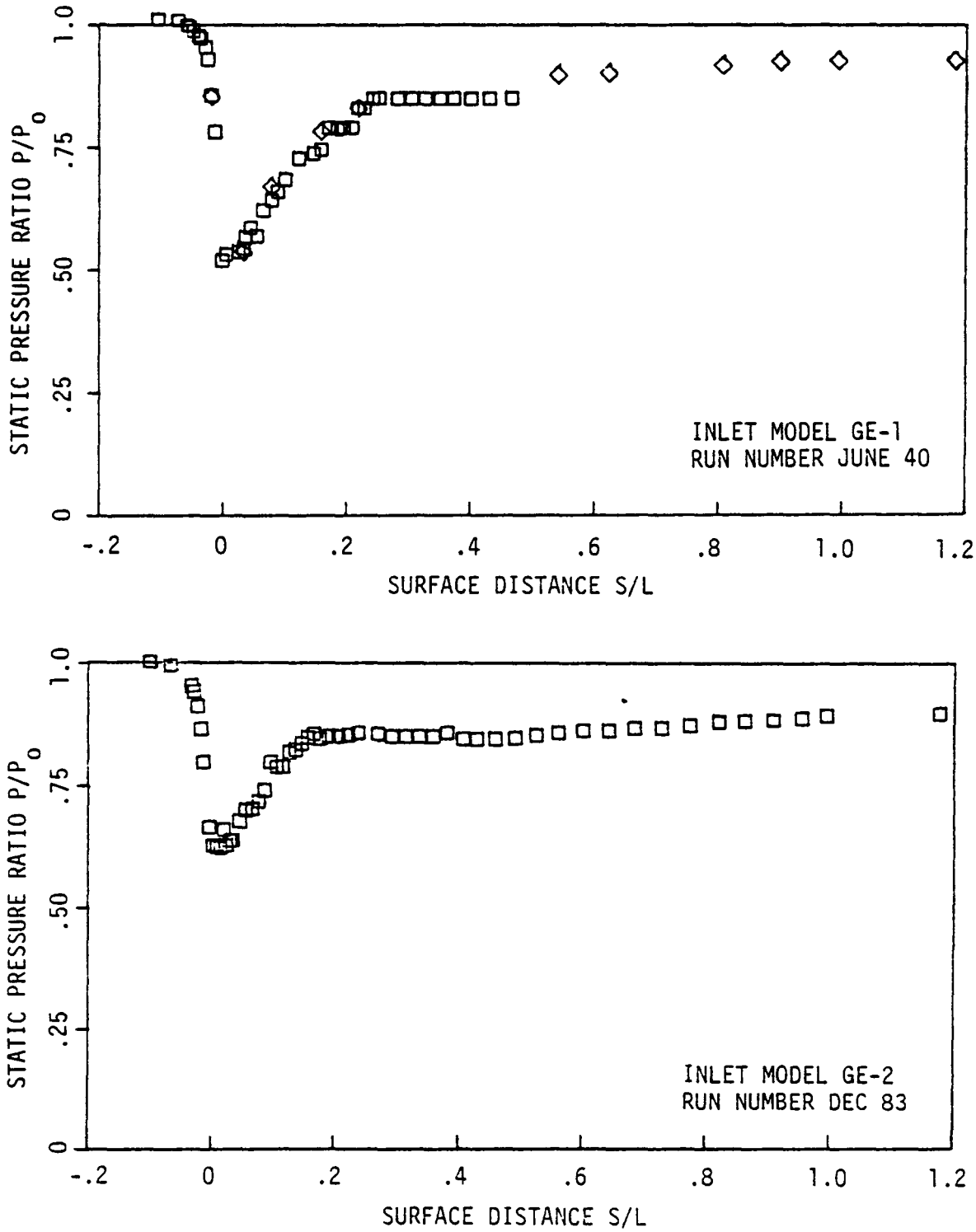

Fig. 25 INLET MODEL WINDWARD SURFACE STATIC PRESSURE DISTRIBUTION: U_∞=150 ft/sec, M_T=0.38, α=30°

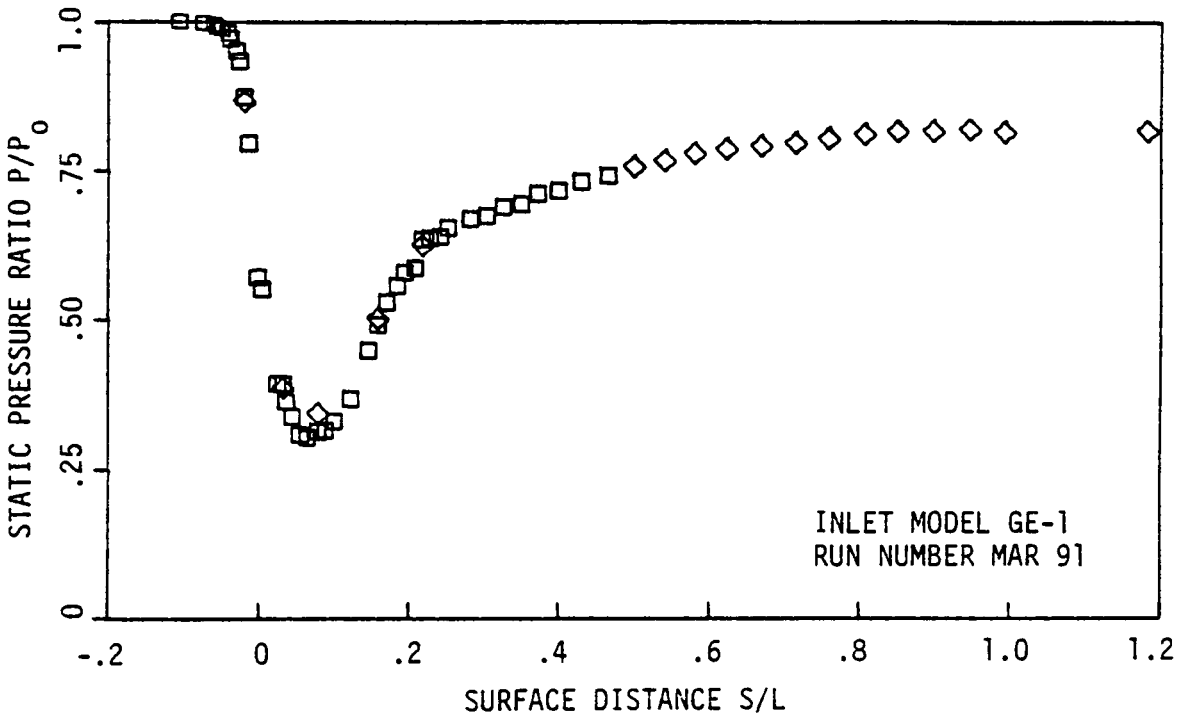

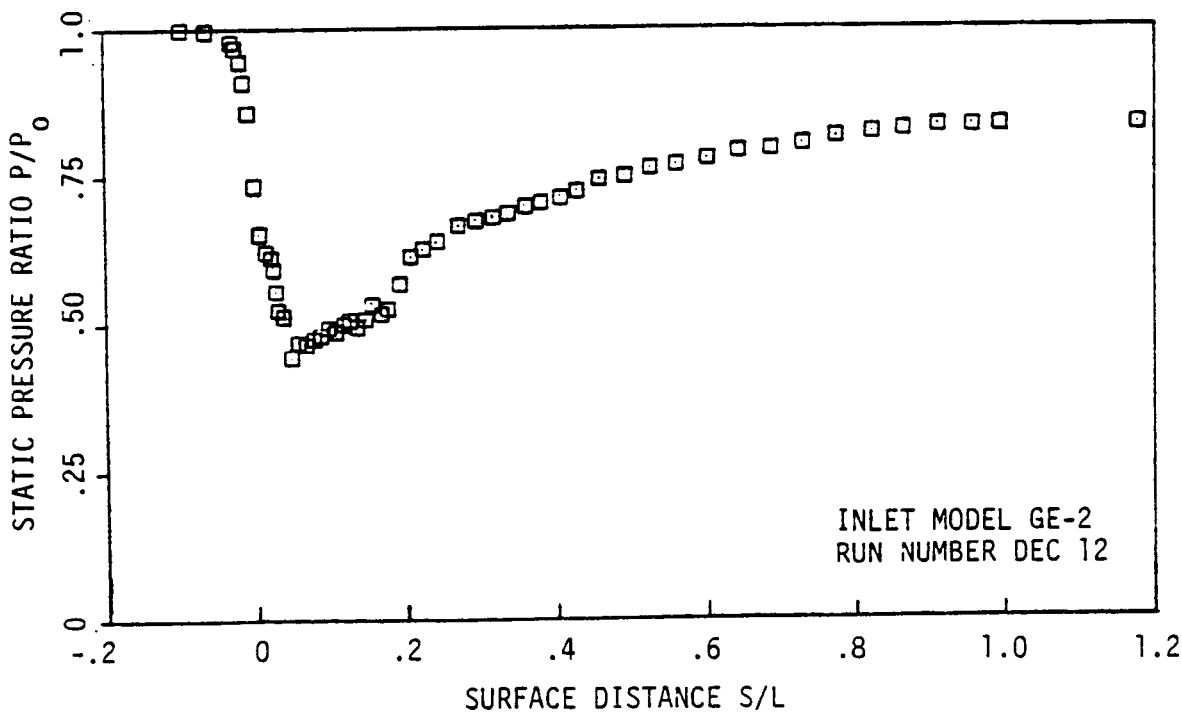

Fig. 26 INLET MODEL WINDWARD SURFACE STATIC PRESSURE DISTRIBUTION:
U_∞=150 ft/sec, M_T=0.73, α=0°

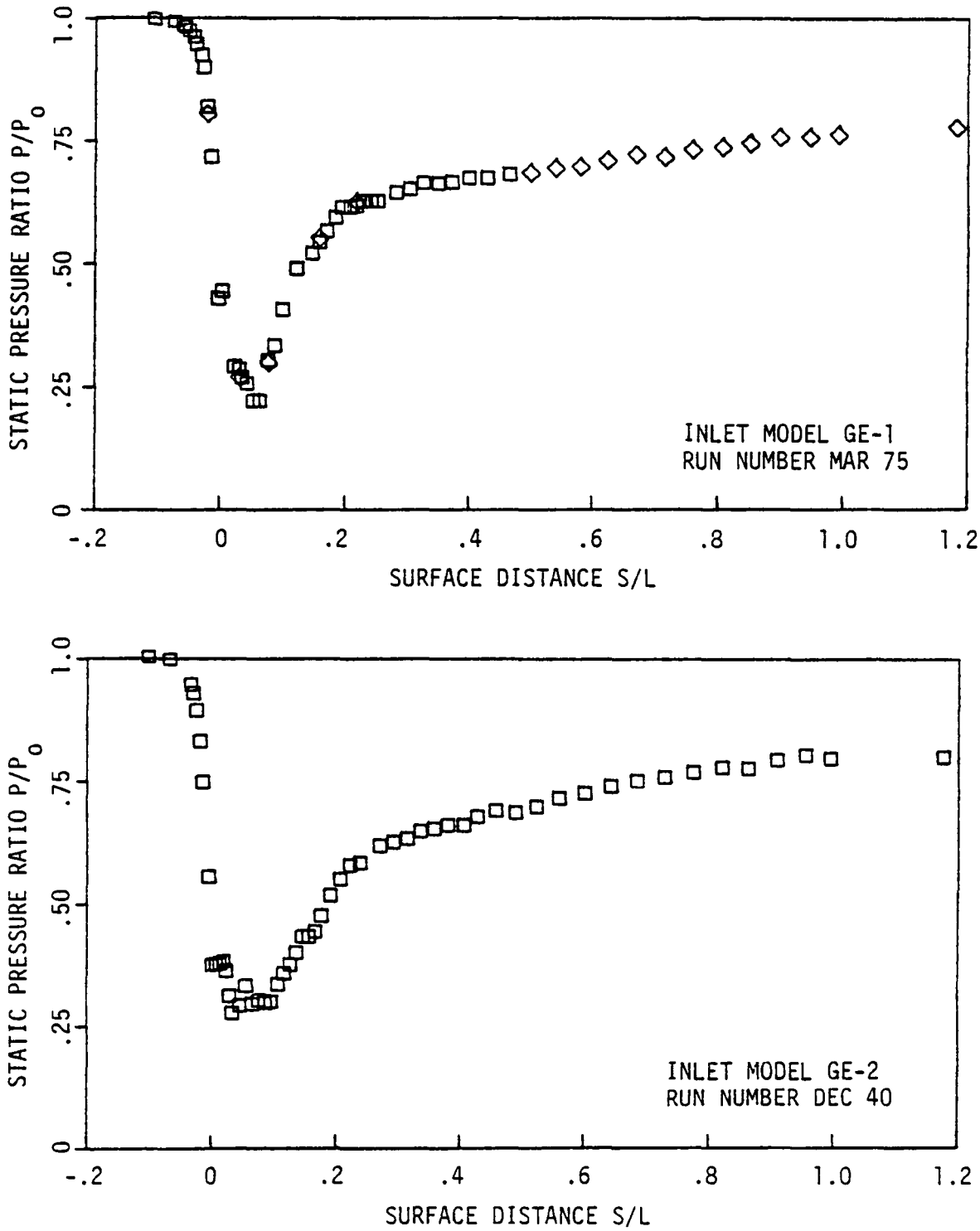

Fig. 27 INLET MODEL WINDWARD SURFACE STATIC PRESSURE DISTRIBUTION: U_∞=150 ft/sec, M_T=0.73, α=15°

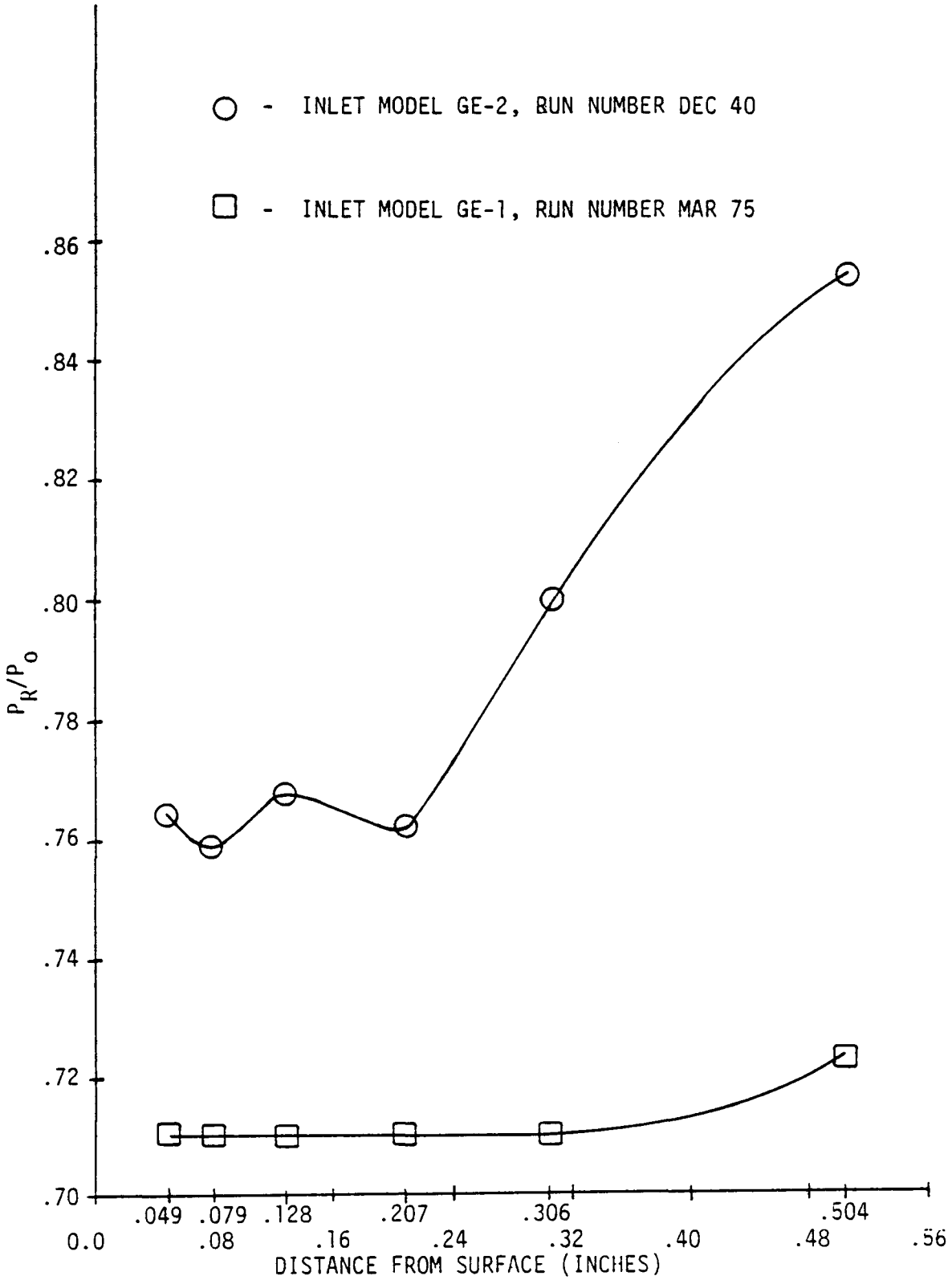

Fig. 28 BOUNDARY LAYER RAKE #2 PROFILE: U_∞=150ft/sec, M_∞=0.73, α=15°

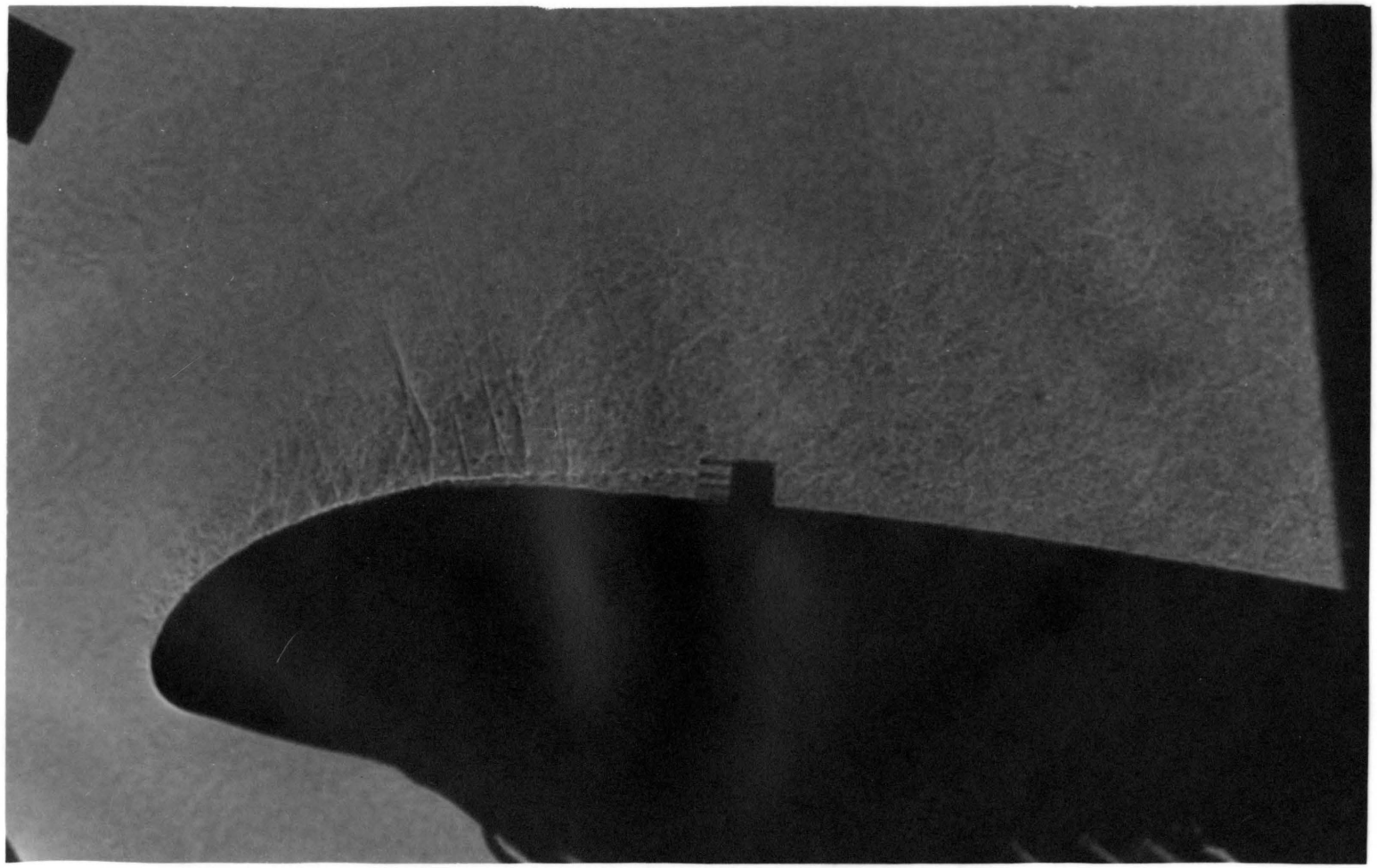

Fig. 29 SHADOWGRAPH PICTURE, INLET MODEL GE-1, RUN NUMBER MAR 75:
U_∞=150 ft/sec, M_T=0.73, α=15°

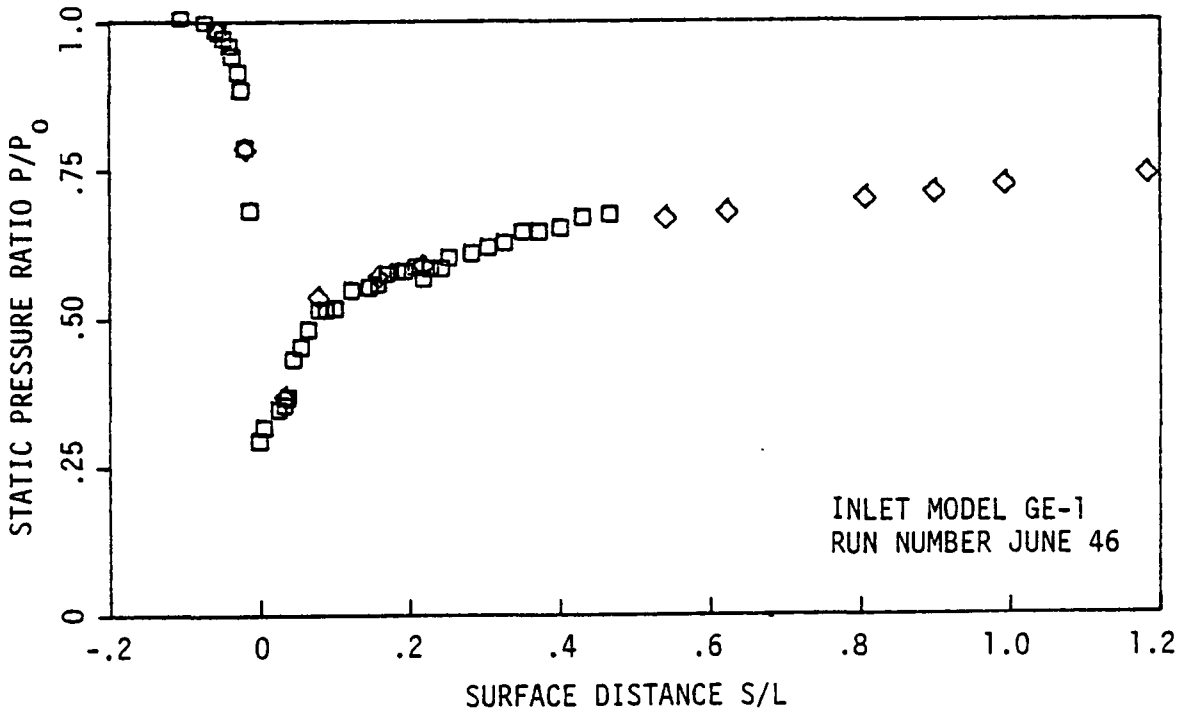

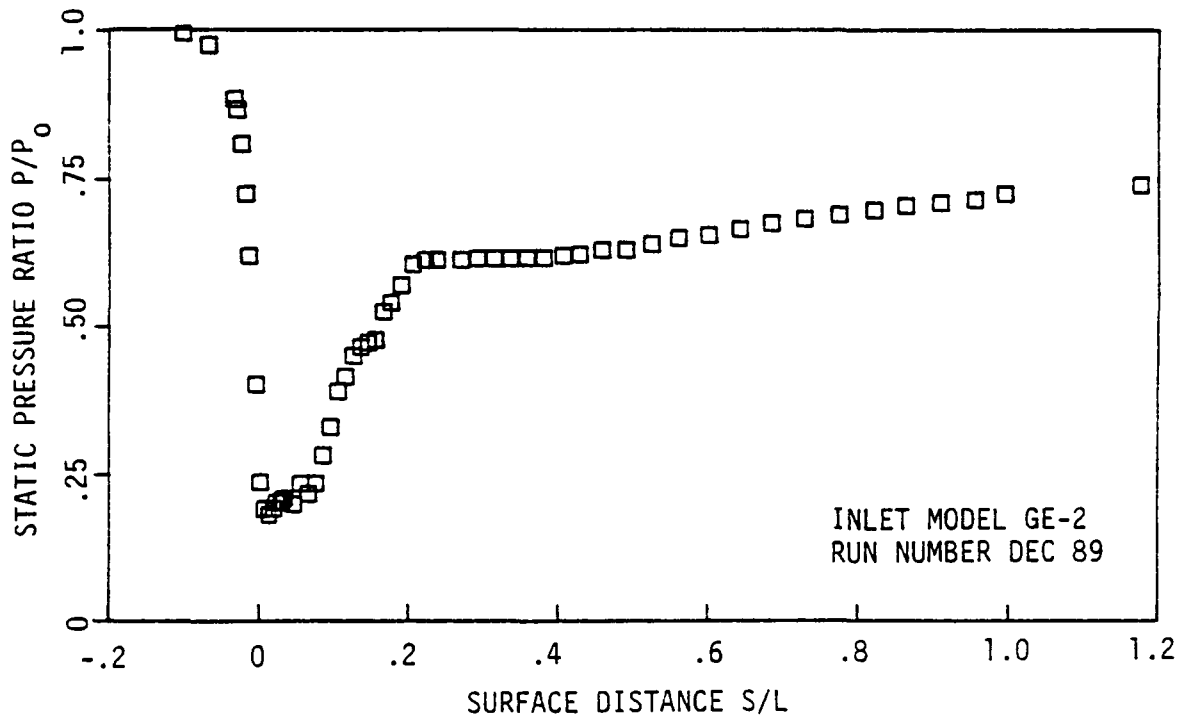

Fig. 30 INLET MODEL WINDWARD SURFACE STATIC PRESSURE DISTRIBUTION:
U_∞=150 ft/sec, M_T=0.73, α=30°

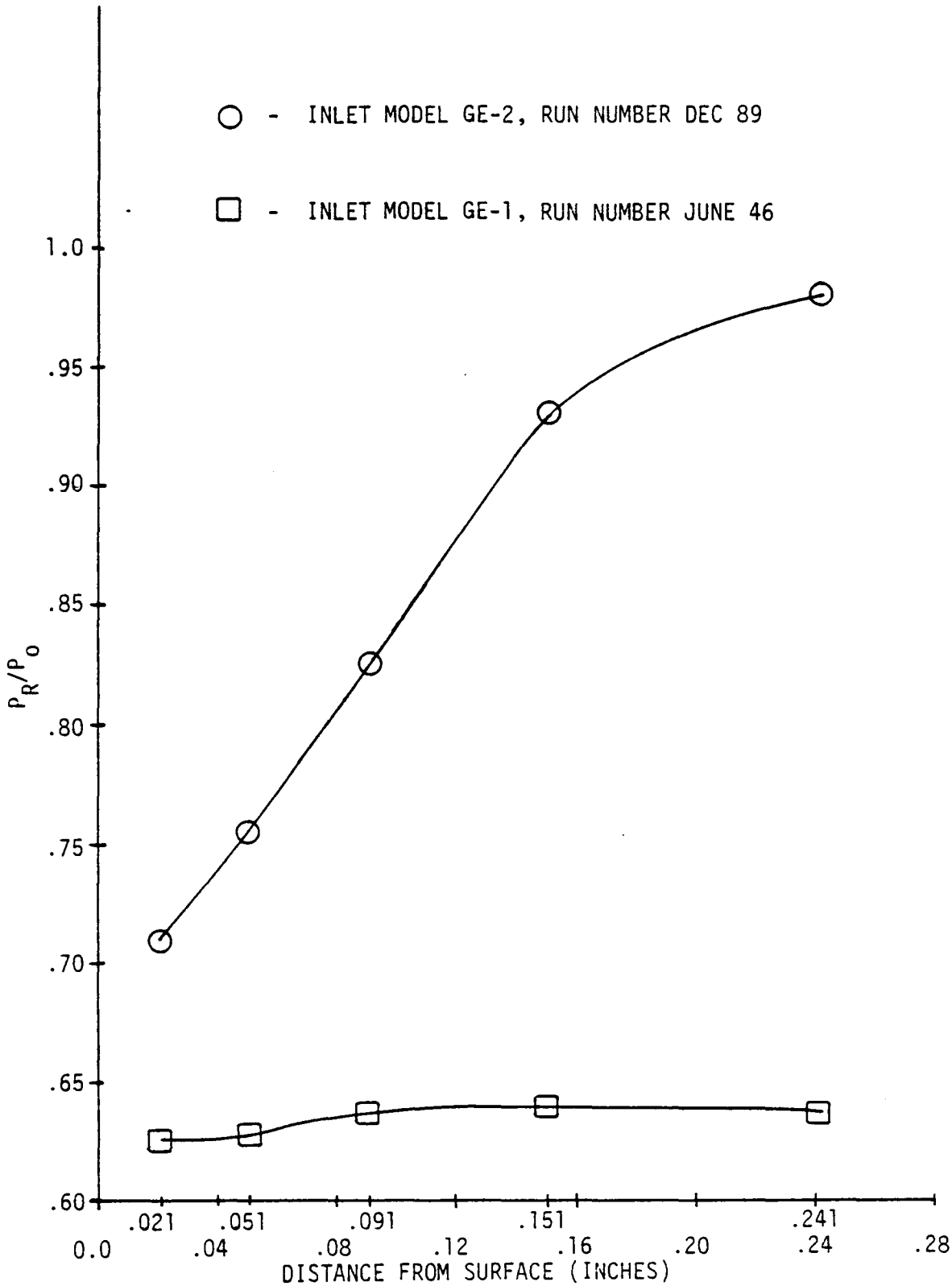

Fig. 31 BOUNDARY LAYER RAKE #1 PROFILE: U_∞=150ft/sec, M_T=0.73, α=30°

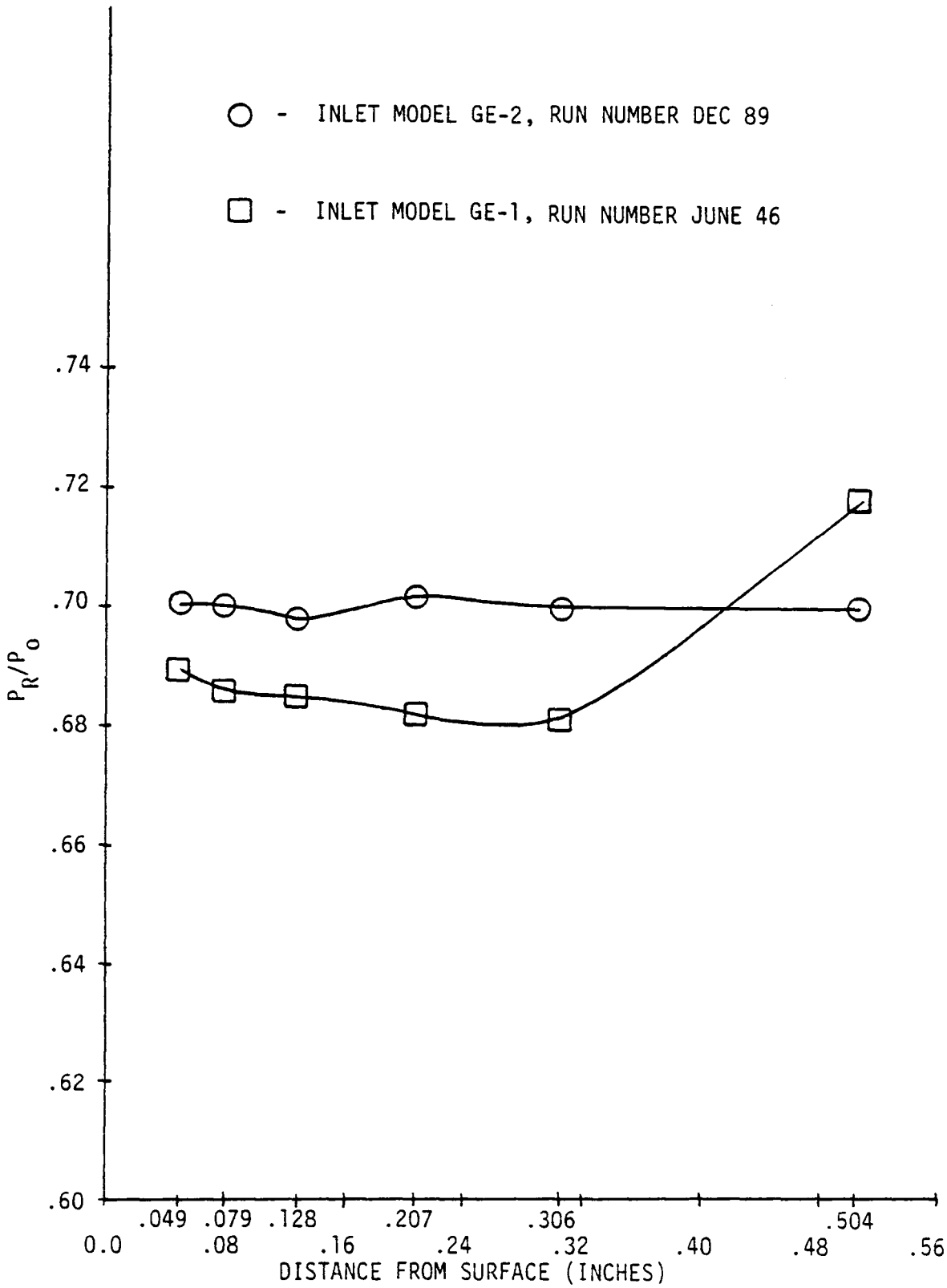

Fig. 32 BOUNDARY LAYER RAKE #2 PROFILE: U_∞=150ft/sec, M_T=0.73, α=30°

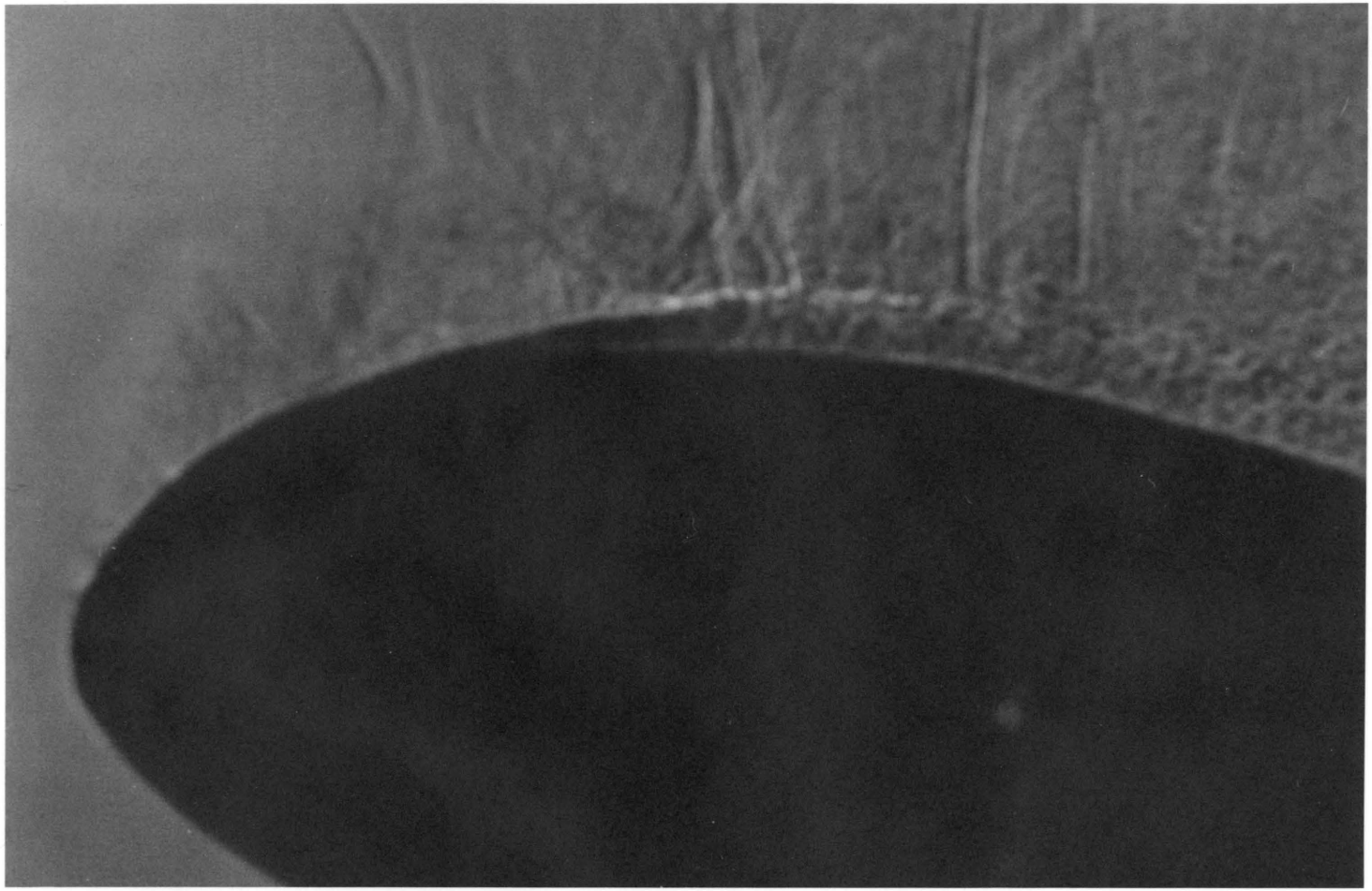

Fig. 33 SHADOWGRAPH PICTURE, INLET MODEL GE-2, RUN NUMBER DEC 89:
U_∞=150 ft/sec, M_T=0.73, α=30°

APPENDIX

1. Induced mass flow rate, $\dot{m}_i$

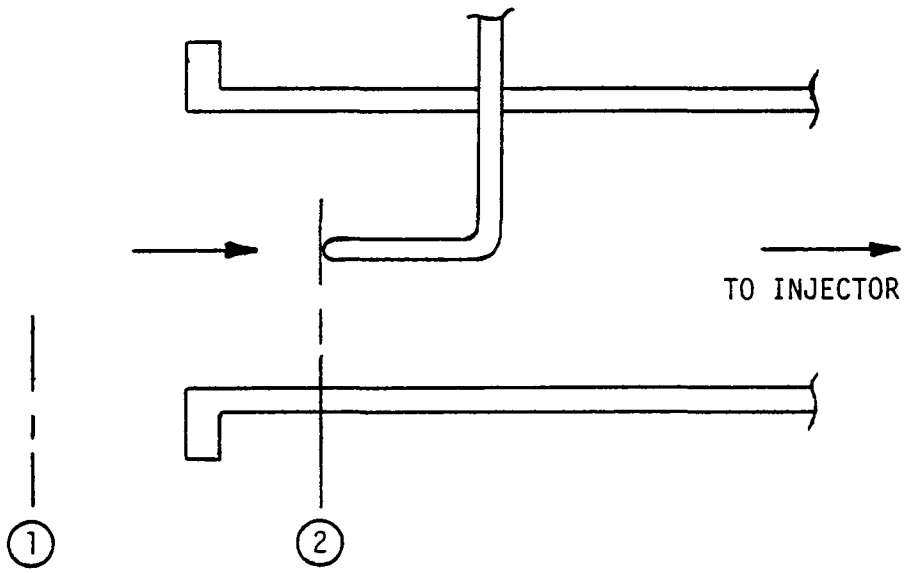

Governing equations are:

Continuity $\dot{m} = \rho_1 u_1 A_1 = \rho_2 u_2 A_2$ (1)

State $P = \rho RT$ (2)

Energy $h_o = c_p T_1 + u_1^2/2g_c = c_p T_2 + u_2^2/2g_c$ (3)

Combining (1), (2) and (3) and assuming u_1 to be very small:

$$\dot{m} = \rho_1 u_1 A_1 = (P_1/RT_1) u_1 A_1 = (P_1/RT_1)(u_2 A_2 \rho_2/\rho_1)$$

$$= (P_1/RT_1) A_2 \sqrt{2g_c c_p (T_1 - T_2)}\ (\rho_2/\rho_1)$$

$$= (P_1/RT_1) A_2 \sqrt{2g_c c_p}\sqrt{T_1\left(1 - \frac{T_2}{T_1}\right)}\left(\frac{P_2}{P_1}\right)(P_1/P_2)^{\frac{\gamma - 1}{\gamma}}$$

$$\dot{m} = (P_1/RT_1)A_2\sqrt{2g_c c_p}\sqrt{T_1}\sqrt{1 - \left(\frac{P_2}{P_1}\right)^{\frac{\gamma-1}{\gamma}}} \quad \frac{P_2}{P_1}\left(\frac{P_1}{P_2}\right)^{\frac{\gamma-1}{\gamma}}$$

$$= (P_1/R\sqrt{T_1})A_2\sqrt{2g_c c_p}\sqrt{1 - \left(\frac{P_2}{P_1}\right)^{\frac{\gamma-1}{\gamma}}}\left(\frac{P_2}{P_1}\right)^{\frac{1}{\gamma}}$$

$$= (P_1/R\sqrt{T_1})A_2\sqrt{2g_c c_p}\sqrt{\left[1 - \left(\frac{P_2}{P_1}\right)^{\frac{\gamma-1}{\gamma}}\right]\left(\frac{P_2}{P_1}\right)^{\frac{2}{\gamma}}}$$

$$= (P_1/R\sqrt{T_1})A_2\sqrt{2g_c c_p}\sqrt{\left(\frac{P_2}{P_1}\right)^{\frac{2}{\gamma}} - \left(\frac{P_2}{P_1}\right)^{\frac{\gamma+1}{\gamma}}}$$

Now since

$$R = c_p - c_v = c_p(1 - c_v/c_p) = c_p\left(1 - \frac{1}{\gamma}\right) = c_p\frac{\gamma-1}{\gamma}$$

Then

$$\frac{\sqrt{c_p}}{R} = \sqrt{\frac{\gamma}{\gamma-1}}\ \frac{1}{\sqrt{R}}$$

Substituting this into the mass flow rate equation:

$$\dot{m} = \sqrt{2g_c}\ A_2\sqrt{\frac{\gamma}{\gamma-1}}\ (P_1/\sqrt{RT_1})\sqrt{\left(\frac{P_2}{P_1}\right)^{\frac{2}{\gamma}} - \left(\frac{P_2}{P_1}\right)^{\frac{\gamma+1}{\gamma}}}$$

Where:

A_2 = cross sectional area of the pipe

P_1 = atmospheric pressure

P_2 = static pressure inside pipe

T_1 = atmospheric temperature

g_c = acceleration due to gravity

γ = specific heat ratio (c_p/c_v)

2. Injected mass flow rate, $\dot{m}_j$

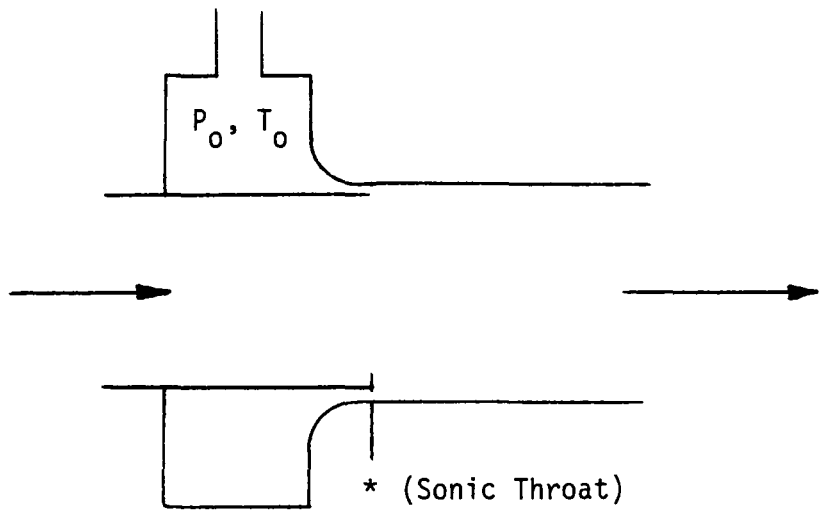

Governing equations are:

Continuity $\dot{m} = \rho^* u^* A^*$ (1)

State $P = \rho RT$ (2)

Combining (1) and (2):

$$\dot{m} = \rho^* u^* A^* = \frac{\rho^*}{\rho_o} \rho_o \sqrt{\gamma R T^*}\, A^*$$

$$= .6339 \frac{P_o}{RT_o} \sqrt{\gamma R \frac{T^*}{T_o} T_o}\, A^* = .6339 \sqrt{\frac{\gamma}{R}} \sqrt{.833} \frac{P_o}{\sqrt{T_o}} A^*$$

Finally:

$$\dot{m} = (.01653)(32.17) \frac{P_o}{\sqrt{T_o}} A^*$$

The vita has been removed from the scanned document

INLET MODEL TESTING FACILITY PREPARATION, INJECTOR CALIBRATION AND PRELIMINARY TESTING OF TWO TWO-DIMENSIONAL INLET MODELS AT HIGH INCIDENCE ANGLES TO STUDY INTERNAL FLOW SEPARATION

by

Daniel Robert Hatfield

ABSTRACT

An experimental study of internal flow separation at high incidence angles for two two-dimensional inlet models is presented. A description of the inlet testing facility includes the injector (which serves to drive the air through the inlet model), its control system, and the Virginia Tech 6-foot subsonic wind tunnel. The geometry of the two inlet models is discussed and the inlet model instrumentation is described. The injector is calibrated in preparation for the inlet model tests and found to exhibit satisfactory performance. Inlet models GE-1 and GE-2 are tested at incidence angles of 0°, 15°, and 30°, and at throat Mach numbers of 0.38, and 0.73. Preliminary data is presented and comparisons show a favorable trend toward delaying internal flow separation for the inlet model which has a thicker lip (higher contraction ratio).